

## CANCER

# Polyamines drive myeloid cell survival by buffering intracellular pH to promote immunosuppression in glioblastoma

Jason Miska<sup>1\*</sup>, Aida Rashidi<sup>1</sup>, Catalina Lee-Chang<sup>1</sup>, Peng Gao<sup>2</sup>, Aurora Lopez-Rosas<sup>1</sup>, Peng Zhang<sup>1</sup>, Rachel Burga<sup>1</sup>, Brandyn Castro<sup>1</sup>, Ting Xiao<sup>1</sup>, Yu Han<sup>1</sup>, David Hou<sup>1</sup>, Samay Sampat<sup>1</sup>, Alex Cordero<sup>1</sup>, Joshua S. Stoolman<sup>3</sup>, Craig M. Horbinski<sup>1</sup>, Mark Burns<sup>4</sup>, Yana K. Reshetnyak<sup>5</sup>, Navdeep S. Chandel<sup>3</sup>, Maciej S. Lesniak<sup>1</sup>

Copyright © 2021  
The Authors, some  
rights reserved;  
exclusive licensee  
American Association  
for the Advancement  
of Science. No claim to  
original U.S. Government  
Works. Distributed  
under a Creative  
Commons Attribution  
NonCommercial  
License 4.0 (CC BY-NC).

Glioblastoma is characterized by the robust infiltration of immunosuppressive tumor-associated myeloid cells (TAMCs). It is not fully understood how TAMCs survive in the acidic tumor microenvironment to cause immunosuppression in glioblastoma. Metabolic and RNA-seq analysis of TAMCs revealed that the arginine-ornithine-polyamine axis is up-regulated in glioblastoma TAMCs but not in tumor-infiltrating CD8<sup>+</sup> T cells. Active de novo synthesis of highly basic polyamines within TAMCs efficiently buffered low intracellular pH to support the survival of these immunosuppressive cells in the harsh acidic environment of solid tumors. Administration of difluoromethylornithine (DFMO), a clinically approved inhibitor of polyamine generation, enhanced animal survival in immunocompetent mice by causing a tumor-specific reduction of polyamines and decreased intracellular pH in TAMCs. DFMO combination with immunotherapy or radiotherapy further enhanced animal survival. These findings indicate that polyamines are used by glioblastoma TAMCs to maintain normal intracellular pH and cell survival and thus promote immunosuppression during tumor evolution.

## INTRODUCTION

Glioblastoma (GBM) is an aggressive primary tumor of the central nervous system (CNS) that is lethal despite the continuous efforts to treat the disease (1, 2). While immunotherapy has become immensely effective for most malignancies, for brain tumors it remains disappointing, in part, because of the immune composition of brain tumors (3). GBM has an infiltration of tumor-associated myeloid cells (TAMCs) and deficiency of T cells that is more robust than any other tumor measured (4). TAMCs are a key driver of immunosuppression and thus a barrier to successful immunotherapy for glioma (5, 6). Recently, there have been large-scale “omics” approaches to understand the immunological composition of glioma and how they influence patient survival (4, 7, 8). These studies have highlighted the importance of myeloid infiltration in glioma and identified targeting of the myeloid compartment as a therapeutic strategy for glioma. For example, we have recently used a TAMC-targeting system that works synergistically with irradiation and chemotherapy to promote survival in multiple animal models of the disease (9). Other groups have also used other TAMC-targeting approaches/therapies to influence the myeloid compartment of brain tumors (10, 11). Moreover, recent studies indicate that modulating metabolic pathways can affect tumor immunity (12–14).

Brain tumors exist in a harsh environment consisting of severe hypoxia (15), extracellular acidification (16–18), and nutrient competition (19, 20). Hypoxia and acidity enhance both cancer aggressiveness (21) and immunosuppression (22, 23). Extracellular acidity (pHe) causes several immunosuppressive aspects of tumor biology. pHe enforces T cell unresponsiveness, and its blockade can promote checkpoint immunotherapy for melanoma (24, 25). Furthermore, recent work highlighted that pHe can directly enforce the immunosuppressive phenotype of macrophages (26). How TAMCs survive the acidic tumor microenvironment (TME) is not fully understood and is addressed in this study.

siveness (21) and immunosuppression (22, 23). Extracellular acidity (pHe) causes several immunosuppressive aspects of tumor biology. pHe enforces T cell unresponsiveness, and its blockade can promote checkpoint immunotherapy for melanoma (24, 25). Furthermore, recent work highlighted that pHe can directly enforce the immunosuppressive phenotype of macrophages (26). How TAMCs survive the acidic tumor microenvironment (TME) is not fully understood and is addressed in this study.

## RESULTS

### TAMCs catabolize arginine to polyamines in brain tumors

To gain insight into this phenomenon, we implanted  $7.5 \times 10^4$  CT-2A glioma cells intracranially into C57/Bl6 mice. After 2 weeks of tumor growth, TAMCs were isolated and compared to splenic myeloid cells using bulk metabolite analysis by liquid chromatography–tandem mass spectrometry (LC-MS/MS; Fig. 1A) and RNA-sequencing (RNA-seq) analysis (Fig. 1B). Using a Gr1-based isolation, we achieved a high purity ( $\geq 89\%$ ) of TAMCs from the brain and myeloid cells from the spleen (fig. S1, A and B) for our downstream analysis. Note that the flow cytometric phenotypes of splenic myeloid cells do not significantly differ from those isolated from the blood in regard to arginase, PD-L1, and percent Ly6C positivity of the CD45<sup>+</sup>CD11b<sup>+</sup> population (fig. S1, C and D). For these reasons, we used splenic myeloid cells as a surrogate for probing peripheral myeloid metabolism. Unbiased examination of bulk metabolites revealed that TAMCs have a significant decrease in arginine with a concomitant increase in its downstream metabolites, ornithine, putrescine, and spermidine (Fig. 1A and table S1). Supporting this observation, we found that enzymes responsible for the catabolism of arginine into ornithine are significantly up-regulated in TAMCs (Tumor Gr1) compared to peripheral myeloid cells (Spleen Gr1) (Fig. 1B). Expression of other well-established myeloid-derived suppressor cells (MDSCs)/tumor-associated

<sup>1</sup>Department of Neurological Surgery, Feinberg School of Medicine, Northwestern University, 676 North St. Clair Street, Suite 2210, Chicago, IL 60611, USA. <sup>2</sup>Metabolomics Core Facility, Feinberg School of Medicine, Northwestern University, 710 N Fairbanks Court, Chicago, IL 60611, USA. <sup>3</sup>Department of Medicine, Feinberg School of Medicine, Northwestern University, 676 North St. Clair Street, Suite 2330, Chicago, IL 60611, USA. <sup>4</sup>Aminex Therapeutics Inc., Epsom, NH 03234, USA. <sup>5</sup>Physics Department, University of Rhode Island, Kingston, RI 02881, USA.

\*Corresponding author. Email: jason.miska@northwestern.edu

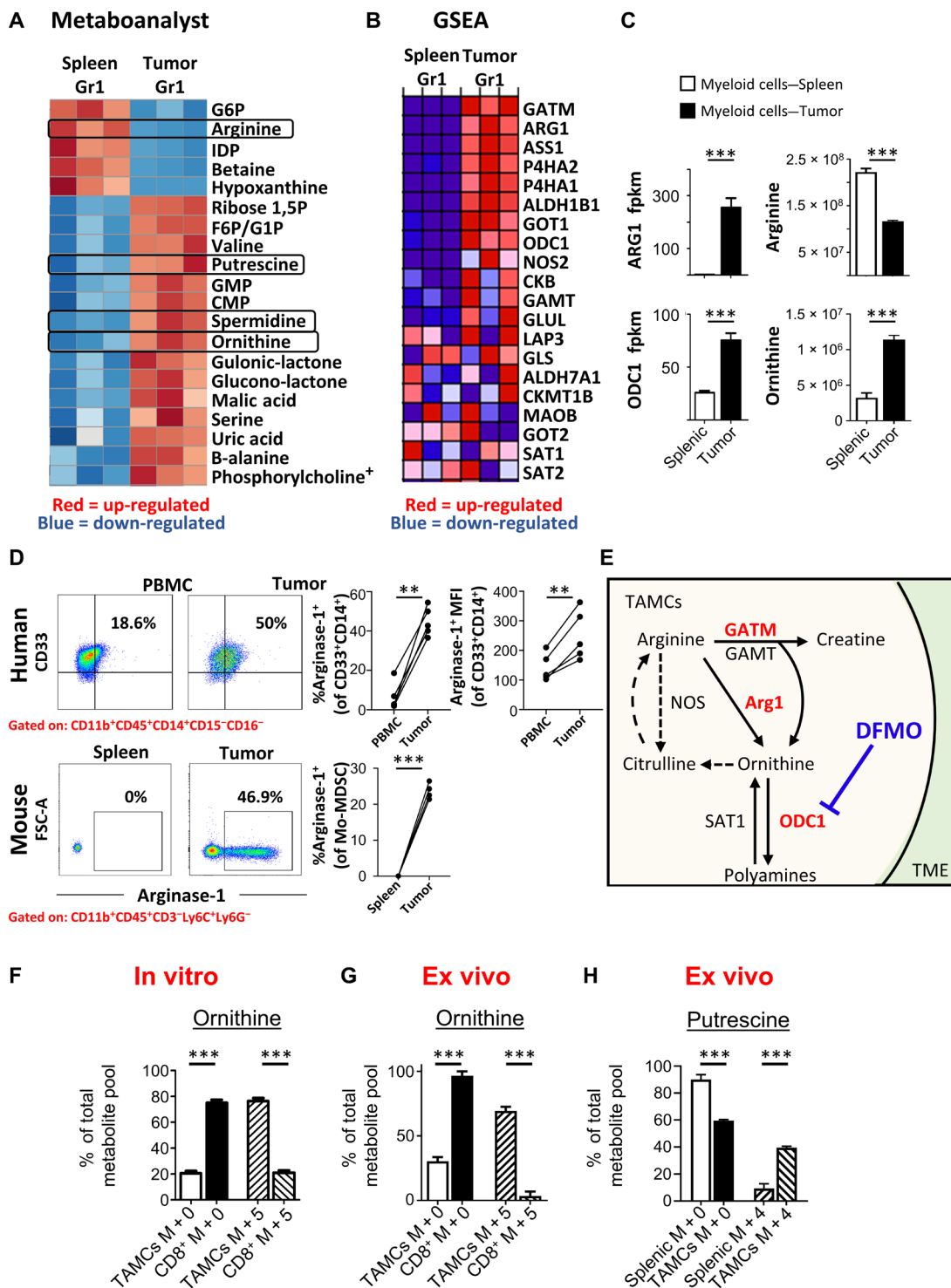


**Fig. 1. TAMCs up-regulate the arginine-polyamine axis in brain tumors.** (A to C) Mice were implanted with  $7.5 \times 10^4$  CT-2A tumor cells, and after 14 days of tumor engraftment, myeloid cells from the brain (TAMCs) and spleen were isolated via Gr1 magnetic bead isolation and analyzed via LC-MS/MS for metabolomics (A) (table S1) and RNA-seq (B). (A) Normalized peak areas of samples were graphed in MetaboAnalyst (74). RNA-seq data were visualized using GSEA heatmap analysis for arginine metabolic genes (B). (C) Left: FPKM values comparing hallmark arginine metabolite genes. Right: Metabolite levels in TAMCs versus peripheral myeloid cells. (D) Flow cytometric expression of arginase-1 in matched peripheral versus tumor myeloid cells of both humans and mice. (E) Schematic of the arginine metabolic pathway. (F) In vitro generated CD8<sup>+</sup> T cells and TAMCs were cultured in <sup>13</sup>C-arginine SILAC medium for 2 hours before LC-MS/MS. (G) TAMC and CD8<sup>+</sup> T cells were isolated from tumor-bearing mice and pulsed ex vivo with <sup>13</sup>C-arginine for 2 hours (4 hours in (H)) and analyzed via LC-MS/MS. (A and B) Each replicate is  $n = 10$  mice pooled per sample, three independent experiments (a total of  $n = 30$  mice). (C) Five matched human and four matched mouse samples were analyzed for arginase-1 expression. (D)  $n = 4$  matched human samples were analyzed for bulk metabolite analysis. Significance was calculated by Student's *t* test: \*\* $P < 0.01$  and \*\*\* $P < 0.001$ .

macrophage (TAM) markers, such as CCR2, PD-L1, and transforming growth factor- $\beta$  (TGF- $\beta$ ), was also enriched in TAMCs, highlighting the validity of this approach (fig. S2A). GSEA (Gene Set Enrichment Analysis) plots generated from RNA-seq data revealed other metabolic pathways up-regulated in TAMCs such as fructose, mannose, and galactose metabolism (fig. S2B). There were also other metabolic pathways down-regulated in the tumor such as nitrogen, glutathione, arachidonic, and purine metabolism (fig. S2C).

Statistical analysis revealed that TAMCs exhibit a 3.27-fold increase in ornithine compared to splenic myeloid cells. There was a concomitant decrease in intracellular arginine levels, indicating robust arginine catabolism (Fig. 1C). Flow cytometric analysis confirmed the up-regulation of arginase-1 in both mouse and human TAMCs compared to peripheral myeloid cells (Fig. 1D). This is consistent with previous studies of arginase-1 expression in TAMCs in glioma (27, 28). We found minimal evidence of critical urea cycle enzymes ornithine transcarbamylase (OTC) and carbamoyl phosphate synthetase 1 (CPS1) or their metabolites (citrulline and carbamoyl phosphate, respectively) in TAMCs or splenic myeloid cells (fig. S2D).

To validate these observations and to understand whether they are myeloid-specific, we first generated TAMCs (9) and CD8<sup>+</sup> T cells in vitro and performed a 2-hour <sup>13</sup>C-arginine relative isotopic incorporation. The M+5 incorporation of TAMCs was  $76.5 \pm 1.2\%$  compared to  $20.9 \pm 0.9\%$  for CD8<sup>+</sup> T cells (Fig. 1F), highlighting the preferential flux of arginine into ornithine by TAMCs. To confirm that this phenomenon occurs similarly in vivo, we performed magnetic bead isolation of TAMCs (Gr1) and CD8<sup>+</sup> T cells (CD8 $\beta$ ) from CT-2A glioma-bearing mice and performed the same ex vivo <sup>13</sup>C-arginine relative isotopic incorporation (Fig. 1G). Again, the results show that M+5 incorporation of TAMCs was  $69.4 \pm 3.2\%$  compared to  $3.4 \pm 3.4\%$  for CD8<sup>+</sup> T cells. These data may suggest that ornithine generation is critical to TAMCs in GBM. Considering that the urea cycle and inducible nitric oxide synthase (iNOS) activity does not appear to be occurring in TAMCs, the only other fate of ornithine is its catabolism to polyamines. The rate-limiting enzyme in this pathway is ornithine decarboxylase 1 (ODC1), which was highly up-regulated in TAMCs (Fig. 1C). A 4-hour ex vivo <sup>13</sup>C-arginine relative isotopic incorporation revealed that TAMCs robustly generated putrescine from arginine, whereas peripheral myeloid cells showed limited capability ( $39.5 \pm 0.9\%$  versus  $9.4 \pm 3.4\%$ , respectively) (Fig. 1H).

### Polyamines promote myeloid-driven immunosuppression

Considering that TAMCs have a preference for generating putrescine from arginine, we analyzed the levels of polyamines in TAMCs compared to CD8<sup>+</sup> T cells in Fig. 2A. The normalized peak area levels of polyamines, particularly putrescine, were greater than fourfold up-regulated in TAMCs ( $2.2 \times 10^6 \pm 1.8 \times 10^5$ ) versus spleens ( $5.6 \times 10^5 \pm 1.9 \times 10^5$ ;  $P < 0.001$ ). Similarly, spermidine levels were 3.82-fold up-regulated in TAMCs ( $1.02 \times 10^8 \pm 6.4 \times 10^6$ ) versus spleens ( $2.7 \times 10^7 \pm 2.5 \times 10^6$ ;  $P < 0.001$ ). In CD8<sup>+</sup> T cells, there was a trend toward a decrease of putrescine in tumors ( $P = 0.1$ ), with an increase in spermidine levels in tumors (0.12-fold increase;  $P < 0.05$ ). The role of polyamines in myeloid immunosuppression has been addressed previously, as Yu *et al.* (29) have revealed that blockade of de novo polyamine generation using difluoromethylornithine (DFMO) inhibits MDSC-mediated suppression of T cells. To determine whether the polyamine pathway is required for immunosuppression, we generated TAMCs as previously described (9) and performed CD8<sup>+</sup> T cell suppressor assays with polyclonal T cells in

Fig. 2B. At 1:2 and 1:4 TAMC:CD8<sup>+</sup> T cells ratios, DFMO pretreatment (added immediately upon differentiation at day 0) caused a significant decrease in TAMC suppressor functions. LC-MS/MS analysis revealed that DFMO pretreatment depletes both putrescine and spermidine from TAMCs (fig. S3A). To determine whether this can influence antigen-specific responses, we performed the same assay using OT-1 CD8<sup>+</sup> T cells and SIINFEKL peptide stimulation for 48 hours in Fig. 2C. Similar to polyclonal cultures, DFMO pretreatment markedly impaired TAMC-induced suppression.

To determine whether DFMO can block polyamine generation in vivo, we implanted mice with CT-2A and, after 5 days of tumor engraftment (which was sufficient time for tumor establishment as verified by neuropathological examination), administered 1% DFMO in their drinking water ad libitum. After 7 days of water treatment, TAMCs were isolated and compared to splenic myeloid cells using LC-MS/MS (Fig. 2D). While splenic myeloid cells showed no changes in polyamine content, TAMCs had significant reductions in their polyamine content. This suggests that de novo polyamine generation is required only within the TME. To understand whether this reduction is specific to the arginine-ornithine-polyamine axis, we performed a 4-hour <sup>13</sup>C-arginine relative isotopic incorporation ex vivo (Fig. 2E). While there was no difference in the amount of <sup>13</sup>C-labeled ornithine in DFMO-treated animals (suggesting that M+5 ornithine incorporation is at steady state), the amount of labeled putrescine was almost entirely diminished in the TAMCs of DFMO-treated mice ( $P < 0.001$ ; Fig. 2E). There was no change in <sup>13</sup>C-labeled putrescine in peripheral myeloid cells, supporting a tumor-specific phenomenon. To address the possibility of steady-state labeling, we performed a <sup>13</sup>C-arginine metabolite flux analysis over multiple time points and found that ornithine flux was reduced in DFMO-treated animals at 1 hour ( $P < 0.001$ ), while it remained steady after 2 hours (fig. S3B). Putrescine labeling occurred beginning at 4 hours of flux in which DFMO-treated animals never had putrescine labeling (fig. S3C). These facts suggest that DFMO treatment stymies arginase activity, while it abolishes ODC1 activity. There was no change in <sup>13</sup>C-labeled urea cycle metabolites, confirming the RNA-seq and bulk metabolomics data (fig. S4). This suggests that the urea cycle/iNOS pathway is inactive in TAMCs in glioma.

We also analyzed the bulk metabolites that significantly changed by DFMO treatment in TAMCs (fig. S5) to determine other effects of polyamine inhibition. We found a broad array of metabolites down-regulated by DFMO treatment that was independent of arginine metabolism, such as *N*-acetylglucosamine, guanosine diphosphate, and glutamine (fig. S5A). Some metabolites were increased by DFMO treatment, such as 2,3-bisphosphoglycerate, deoxyguanosine, pantothenic acid, and others (fig. S5B). This suggests that polyamine inhibition exerts effects beyond just the arginine metabolic pathway.

### Polyamine blockade enhances antitumor immunity in GBM

We next sought to understand whether DFMO can be used to promote animal survival in our murine models of glioma. After 5 days of tumor establishment, mice with ad libitum access to 1% DFMO drinking water showed a significant enhancement in survival (median survival of 20 days in controls versus 33 days in DFMO treatment;  $P < 0.001$ ), as indicated in Fig. 3A. Considering that ODC1 is broadly expressed in most brain tumors and inversely correlated with patient survival (fig. S6), there is a possibility that inhibition of ODC1 may directly influence the growth of tumor, rather than antitumor immunity (30). To rule out this possibility, we performed the same

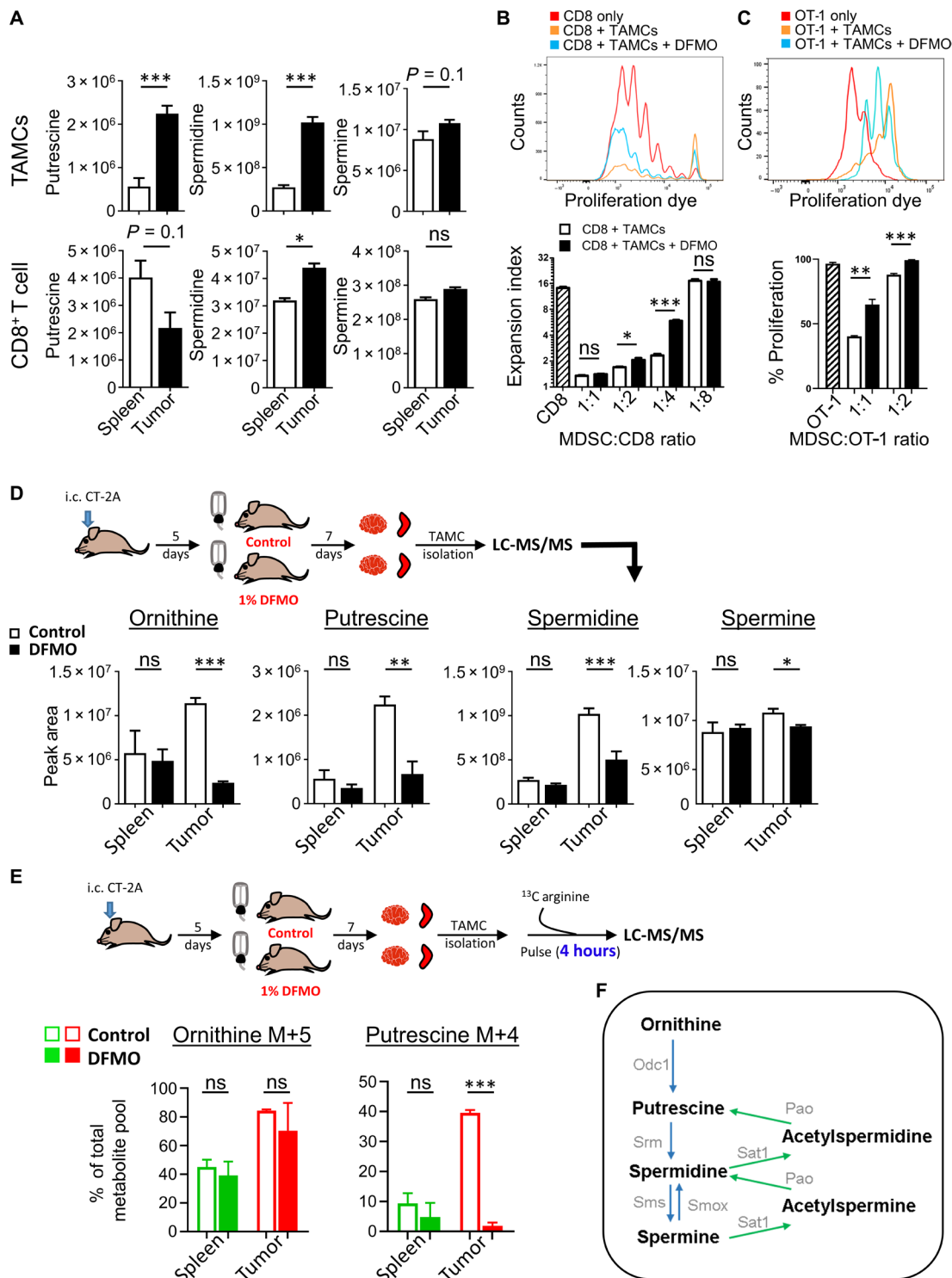


**Fig. 2. Polyamines accumulate in TAMCs in GBM and can be efficiently depleted in vivo.** (A) Mice were implanted with  $7.5 \times 10^4$  CT-2A tumor cells, and after 14 days of tumor engraftment, TAMCs were isolated via Gr1 magnetic bead isolation and CD8<sup>+</sup> T cells were isolated via CD8<sup>+</sup> magnetic bead isolation. (B) In vitro generated TAMCs pretreated with DFMO before being cocultured with decreasing ratios of splenic CD8<sup>+</sup> T cells labeled with CellTrace Violet dye. (C) The same assay was performed using OT-1 T cells stimulated with SIINFEKL peptide. Forty-eight (C) and 72 (B) hours after coculture, T cell proliferation was analyzed via flow cytometric analysis. (D and E) Mice were implanted with  $7.5 \times 10^4$  CT-2A tumor cells, and after 5 to 6 days of tumor engraftment, 1% DFMO water was supplied ad libitum to experimental mice. After 7 days of DFMO water treatment, TAMCs were magnetically isolated for bulk metabolomics (D) or pulsed in vitro with <sup>13</sup>C-arginine for 4 hours before metabolite isolation (E). (F) Schematic overview of polyamine metabolism. (A, D, and E) Each sample is  $n = 8$  to 10 mice pooled per sample, three pooled samples per group. (B and C) Suppressor assays were carried out with  $n = 3$  per each ratio tested, representative of two independent experiments. All statistics in this figure were analyzed by unpaired Student's *t* tests: \* $P < 0.05$ , \*\* $P < 0.01$ , and \*\*\* $P < 0.001$ ; ns, not significant. All LC/MS data were normalized to total ion count (TIC). i.c., intracranial.



survival experiment in RAG-1 knockout (KO) mice (lacking T and B cells) and found a minimal change in the survival of mice (median survival of 16 days in controls versus 19 days in DFMO treatment;  $P < 0.001$ ) (Fig. 3B). This strongly supports the hypothesis that DFMO perturbs the immunosuppressive microenvironment of glioma, not glioma cells themselves. Flow cytometric analysis demonstrated that the myeloid compartment (including microglia) in the tumor of DFMO-treated RAG-1 KO mice significantly up-regulates tumor necrosis factor- $\alpha$  (TNF $\alpha$ ; fig. S7A), while other cytokines were unaffected. Notably, after 1 week of DFMO treatment in immunocompetent animals, a significant reduction in the myeloid:CD8<sup>+</sup> T cell ratio was observed as shown in Fig. 3C. Consistent with our metabolic data, DFMO appears to specifically target M-MDSCs (monocytic MDSCs)/monocytes, microglia, and TAMs in the tumor, as PMN-MDSCs (polymorphonuclear MDSCs)/neutrophils and all measured T cell subsets were unaffected (Fig. 3D). DFMO treatment caused a significant reduction in arginase-1 expression within the M-MDSC/monocyte compartment, suggesting that DFMO causes perturbation of the entire arginine metabolic pathway (Fig. 3C). The gating strategy of this analysis can be found in fig. S8 (A and B). To validate the flow cytometric data, immunofluorescence was performed on tumor tissues harvested from control and DFMO-treated mice (Fig. 3, E and F). Our data, again, show a significant decrease in CD11b<sup>+</sup> cells ( $P < 0.04$ ) and CD11b/CD8 ratio ( $8.1 \pm 0.7$  in controls compared to  $2.4 \pm 0.3$  in DFMO-treated brains;  $P < 0.001$ ) in the tumor with a concomitant increase in CD8<sup>+</sup> cells ( $19 \pm 2$  cells per 20 $\times$  field in controls compared to  $49 \pm 4.6$  in DFMO-treated brains;  $P < 0.001$ ).

DFMO administration in another syngeneic model of glioma (GL-261) also revealed a significant improvement in animal survival (fig. S9A). In this model, we observed a survival benefit (median survival of 20 days in control and 24 days in DFMO treatment;  $P < 0.05$ ; fig. S9A), a reduction of TAMC/T cell ratios ( $P < 0.07$ ; fig. S9B), a down-regulated arginase expression ( $P < 0.01$ ; fig. S9C), and a lower abundance of M-MDSC/monocytes ( $P < 0.05$ ; fig. S9E) with DFMO administration. Marked differences were observed between the two models. In GL-261 model, there were significant increases in CD8/CD4 ratio with DFMO administration ( $0.8 \pm 0.05$  in controls compared to  $1.3 \pm 0.14$  in DFMO-treated brains;  $P < 0.01$ ; fig. S9D), while we did not observe differences in microglial populations (fig. S9E). This suggests that there might be a model-to-model variation in the way polyamine blockade influences anti-GBM immunity; TAMC perturbation is a common effect.

Polyamines are ubiquitous in nature and have been ascribed to many roles in cells. A seminal study shows that polyamines are required for the proliferation of all mammalian cells (31). To this end, we sought to determine whether TAMCs are generating polyamine to fuel their intratumoral proliferation (Fig. 3G). While there was no change in the Ki-67 expression in TAMCs, Ki-67 was significantly up-regulated in T cell subsets measured in the brain of DFMO-treated mice ( $P < 0.05$ ). However, there was no change in cytokine expression in T cells of DFMO-treated animals, suggesting that other mechanisms of immunosuppression were still functional in these mice (fig. S8, C and D). We observed that although pretreatment with DFMO decreased TAMC/T cell ratios in vivo, it largely up-regulated the expression of PD-L1 on TAMCs in vivo (Fig. 4A) and in vitro (Fig. 4B). Supplementation of TAMCs with exogenous putrescine was able to rescue this up-regulation. This suggests that checkpoint molecules are still functioning in the context of DFMO treatment.

To understand whether DFMO can be used to potentiate immunotherapy, we administered anti-PD-L1 therapeutic antibody together with DFMO treatment in mice and found an additive effect on animal survival (median survival of 26 days in anti-PD-L1 treatment, 30 days in DFMO treatment, and 45 days in the combination group;  $P < 0.001$ ) (Fig. 4C). Combinatorial therapy using anti-PD-1 also increased animal survival (Fig. 4D). As previous work has shown that polyamines can protect GBM from the antitumor effects of radiotherapy (32), we also treated mice with DFMO and radiotherapy (3 Gy  $\times$  3 days), which also resulted in combinatorial survival benefit in mice (Fig. 4E). As the CT-2A model is normally resistant to checkpoint blockade, these data highlight the importance of myeloid cells in promoting the efficacy of both checkpoint immunotherapy and radiotherapy. To examine the immunological effects of combinatorial therapy, we implanted mice with GL-261 tumors overexpressing ovalbumin (OVA) and followed up with treatment of anti-PD-L1, DFMO, or combination starting at 1 week after implantation. One week after therapeutic administration, using tetramer staining, we found an increase in OVA-specific T cells within the tumors of combinatorial-treated animals ( $P < 0.05$ ; Fig. 4, F and G). This suggests that DFMO and checkpoint administration promotes antigen-specific T cell recruitment to brain tumors.

### Polyamines buffer the intracellular pH of TAMCs

We next sought a mechanistic understanding as to why TAMCs have a preference for generation of polyamines in brain tumors. We explored the possibility that as polyamines are highly basic compounds (33), perhaps they are playing a role in TAMC survival in the acidic and hypoxic glioma microenvironment. To determine whether this brain tumor model has an acidic environment, we implanted mice with CT-2A tumors and, 14 days after engraftment, injected mice intravenously with the extracellular pH-sensing probe pHLIP (pH-low insertion peptide) labeled with fluorescent dye Cy5.5 (pHLIP-Cy5.5) and compared to mice without tumors (Fig. 5A). The pHLIP probe only inserts into the membrane of cells within acidic extracellular environments, while it will wash out of pH neutral tissues (34). IVIS imaging demonstrated a strong signal only within tumor-bearing brains but minimal detection in nontumor brains ( $2.03 \times 10^7 \pm 8.14 \times 10^6$  versus  $1.3 \times 10^6 \pm 2.22 \times 10^5$  maximum radiance in tumors compared to controls, respectively;  $P < 0.001$ ) or spleens. This shows that brain tumors generate an extracellular acidic milieu.

We next determined whether polyamines endow TAMCs the ability to survive under conditions of pHe (Fig. 5, B and C). To test this hypothesis, we generated TAMCs in vitro and then cultured for additional 48 hours under pH 6.7 condition. Unexpectedly, DFMO pretreatment caused significant necrosis of TAMCs in the context of acidity but not controls ( $21.1 \pm 1.62\%$  versus  $2.2 \pm 0.36\%$ , respectively;  $P < 0.001$ ). To highlight that polyamines are critical for preventing intracellular acidity-induced cell death, we added putrescine back to our TAMC cultures during DFMO treatment, which was able to rescue TAMC cell death under conditions of pHe. To observe this phenomenon in vivo, we treated mice with DFMO and performed flow cytometry using the pH-sensitive dye pHrodo to measure intracellular pH in TAMCs. pHrodo Red AM dye is taken by cells and activated by low pH, of which the fluorescence intensity increases along with the decreased pH (35). Measurement of normalized pHrodo revealed a significant increase of fluorescence in TAMCs of tumor-bearing mice treated with DFMO that did not

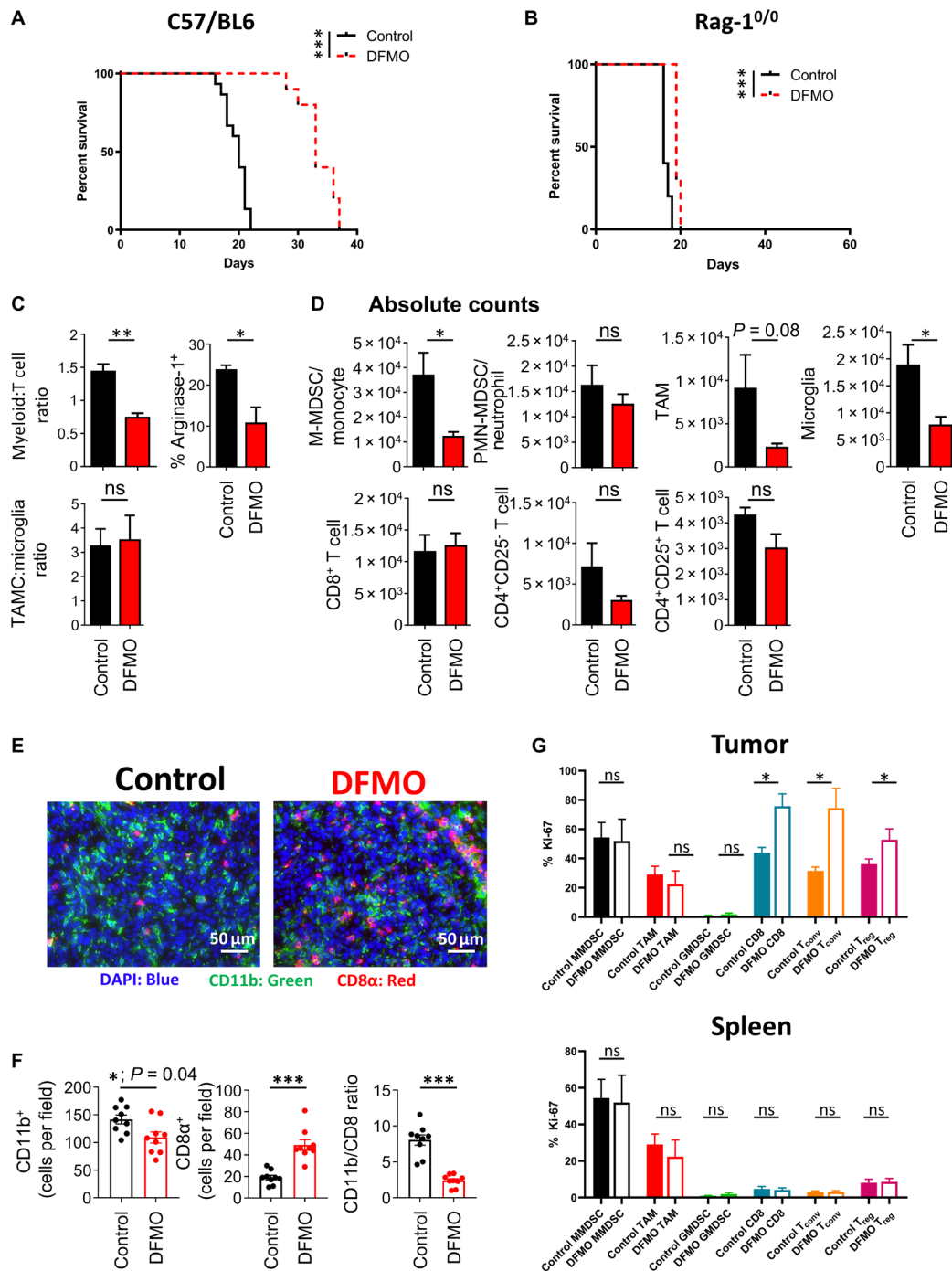


**Fig. 3. Polyamine depletion promotes T cell-driven antitumor immunity in GBM.** C57/BL6 (A) or Rag1<sup>0/0</sup> (B) mice were implanted with  $7.5 \times 10^4$  CT-2A tumor cells, and after 5 to 6 days of tumor engraftment, 1% DFMO water was given. Animal survival was then measured and graphed. (C and D) Mice were implanted with  $7.5 \times 10^4$  CT-2A, administered DFMO ad libitum at day 5, and analyzed via flow cytometry 5 days after DFMO treatment. (C) Ratio of myeloid to T cells; monocyte expression of arginase-1 was calculated. (D) Absolute numbers of myeloid and T cell subpopulations in CT-2A tumor-bearing animals with or without DFMO administration. (E and F) Brains from controls or mice treated with DFMO were harvested and flash-frozen before immunofluorescence was performed using CD11b–Alexa Fluor 488 and CD8 $\alpha$ -PE. (G) Ki-67 expression of all major immune subsets in the tumor compared to the spleen of tumor-bearing mice treated with 1% DFMO in their drinking water as in (C) and (D). (A and B)  $n = 10$  mice per group were used (5 male and 5 female per group, all age-matched at 6 to 8 weeks of age), representative of four experiments in (A) and two experiments in (B). (C, D, and G)  $n = 4$  to 5 mice per group were analyzed and are representative of two independent experiments for each panel. (F)  $n = 4$  mice per group were blindly counted for cellular infiltration. (A and B) Significance was calculated using log-rank analysis followed by Bonferroni correction. (C, D, F, and G) Statistics were calculated via unpaired Student's *t* test: \* $P < 0.05$ , \*\* $P < 0.01$ , and \*\*\* $P < 0.001$ . DAPI, 4',6-diamidino-2-phenylindole; T<sub>conv</sub>, conventional T cell; T<sub>reg</sub>, regulatory T cell.

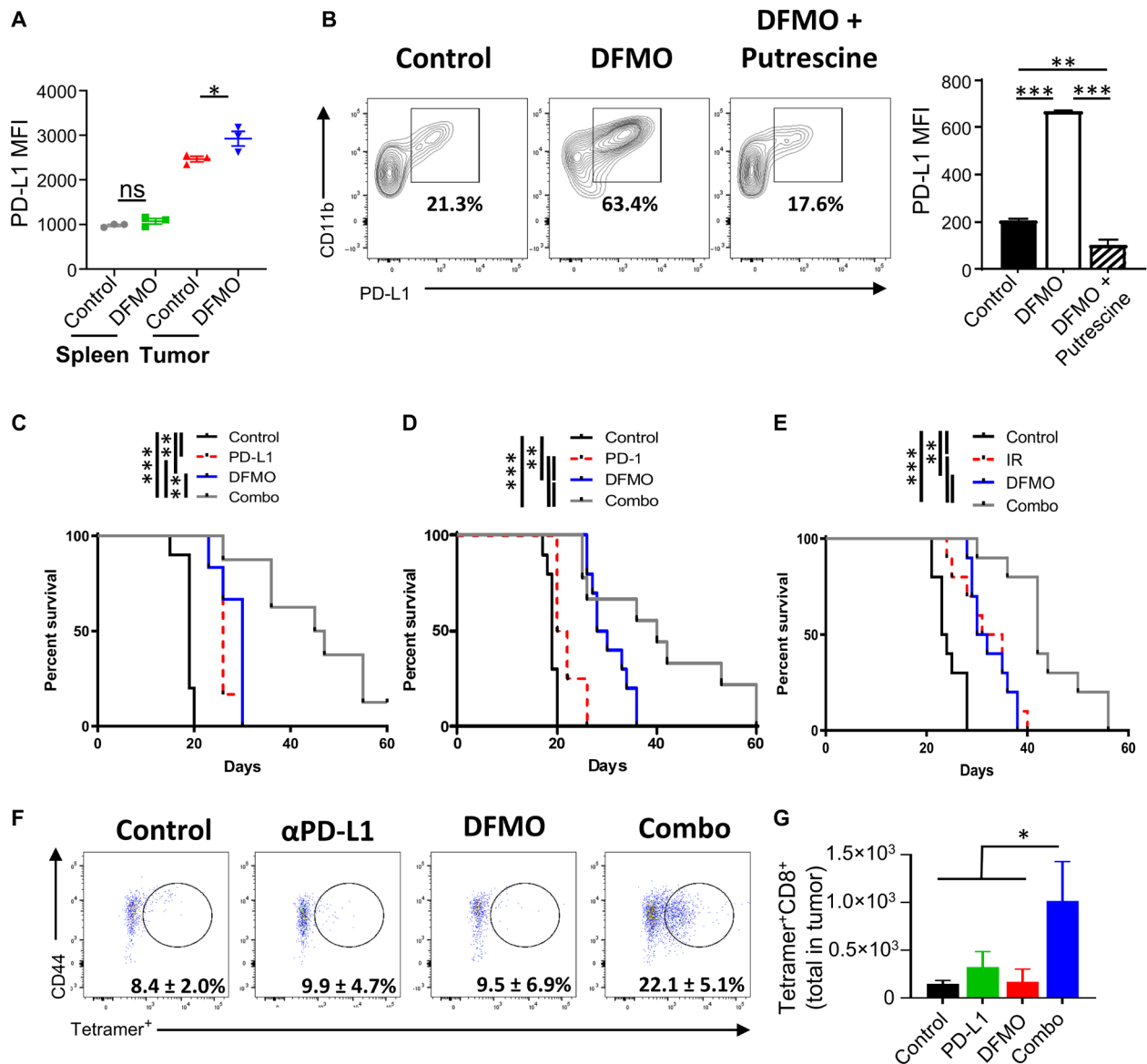


**Fig. 4. Polyamine inhibition promotes multiple different therapies for GBM.** (A) Mice were implanted with  $7.5 \times 10^4$  CT-2A, pretreated with DFMO, and analyzed for PD-L1 MFI expression. (B) TAMCs were generated in vitro in the context of DFMO or DFMO + putrescine, and PD-L1 expression was analyzed after 7 days of differentiation. (C) The same DFMO schema was used in combination with anti-PD-L1 treatment (or treated with monoclonal antibody alone), and animal survival was measured. (D) Seven days after tumor implantation, mice were treated with anti-PD-1 (every 3 days, 10 mg/kg) or combination therapy, and survival was analyzed. (E) Seven days after tumor implantation, mice were treated with DFMO, 3  $\times$  3-Gy irradiation (IR), or combination. (F and G) GL-261 ( $2 \times 10^5$ ) overexpressing OVA were implanted intracranially into mice that were then treated with PD-L1, DFMO, or combinatorial treatment. Brains were harvested and stained for tetramer positivity. (A and B) Data are  $n = 3$  per group representative of two independent experiments. Survival curves were performed  $n = 8$  (C) and  $n = 10$  (D and E) mice per group. Five male and five female mice per group were analyzed in (D) and (E);  $n = 4$  per gender in (C), all age-matched at 6 to 8 weeks of age. (F and G)  $n = 5$  per group were analyzed. Significance in (C) to (E) was calculated using log-rank analysis followed by Bonferroni correction. Significance in (A) and (B) and (F) and (G) was calculated by one-way analysis of variance (ANOVA), followed with a Tukey's post hoc test: \* $P < 0.05$ , \*\* $P < 0.01$ , and \*\*\* $P < 0.001$ .

occur in the spleen (Fig. 5D). Accordingly, the mean fluorescence intensity (MFI) of pHrodo was significantly increased in TAMCs of DFMO-treated mice ( $1788 \pm 157$  arbitrary units in control versus  $2179 \pm 53$  DFMO treated;  $P < 0.05$ ) (fig. S9F), indicating that polyamines are generated within TAMCs to maintain normal intracellular pH and promote survival within the acidic TME. We further validated these findings by generating TAMCs in vitro under DFMO or DFMO + putrescine supplementation, labeled them with

pHrodo, and monitored fluorescence change under acidic pHs over time using the InCyte imaging platform (Fig. 5, E and F). Comparison of treatments across lowering pH revealed that DFMO significantly promotes intracellular acidity in TAMCs that is rescued by putrescine pretreatment (Fig. 5F). Thus, TAMCs treated with DFMO are unable to maintain a neutral intracellular pH under acid stress, whereas controls and putrescine rescue could better handle acid stress. Excessive acidification hinders glycolytic metabolism.

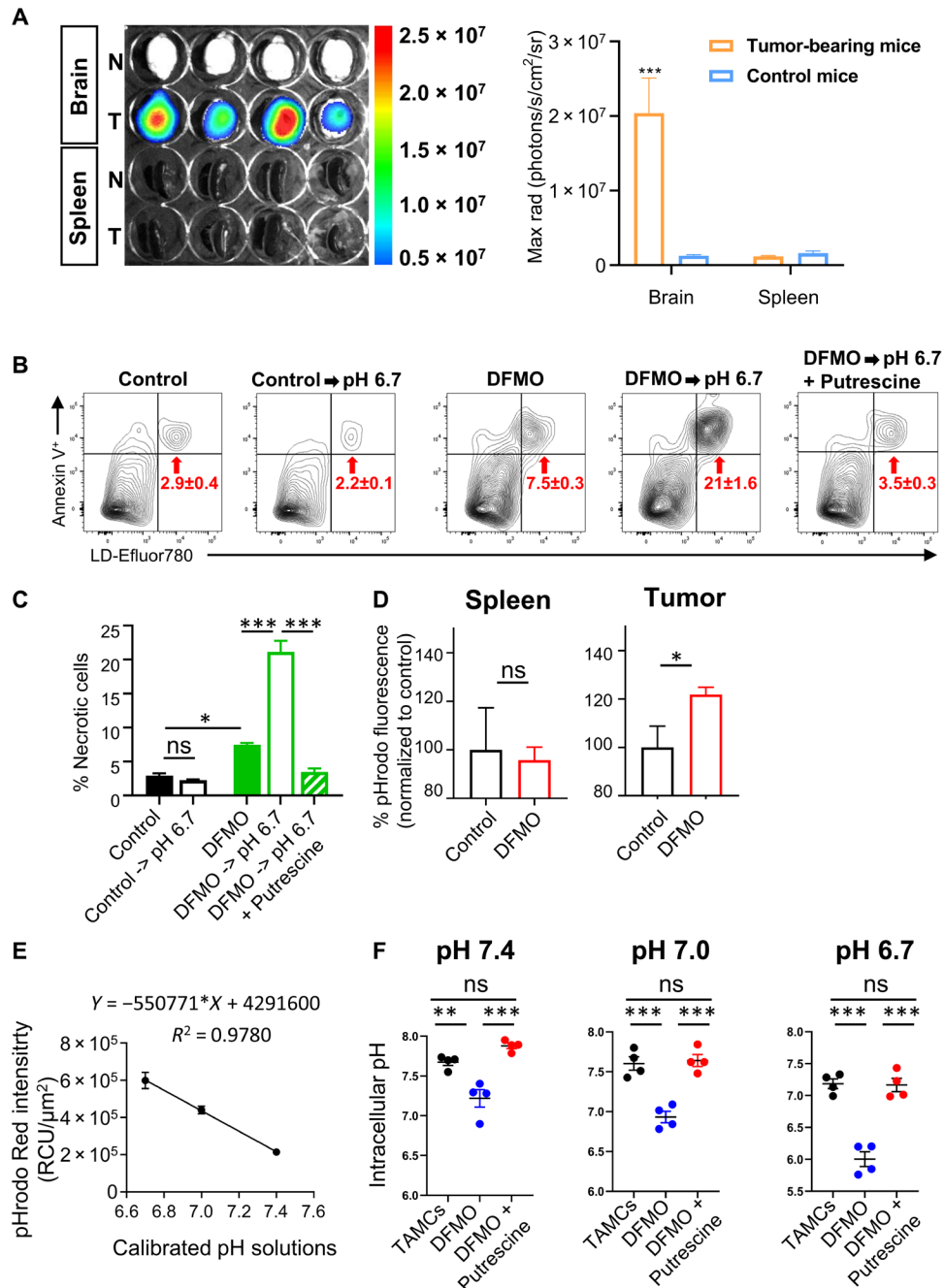


**Fig. 5. Polyamines promote the metabolism and survival of TAMCs by regulating acidic stress produced by the tumor microenvironment.** (A) Mice were implanted with tumors or phosphate-buffered saline (PBS) and, after 14 days, injected with 100 μM pHILIP-Cy5.5 dye via intravenous injection. Twenty-four hours after injection, brains and spleen were quantified using a spectral imaging system. (B and C) TAMCs were generated in the context of DFMO or in DFMO with exogenous putrescine. After 6 days of differentiation, cells were lifted and replated into complete RPMI buffered to an acidic pH. Forty-eight hours after replating, flow cytometric analysis was performed to determine apoptosis/necrosis of TAMCs. (D) Spleens and tumor-infiltrating lymphocytes from controls or DFMO-treated animals were stained with pHrodo Red AM intracellular pH dye. (E) Intracellular pH was determined by generation of pH standard curve. RCU, red calibrated unit. (F) TAMCs were generated under control conditions and pretreated with DFMO or DFMO + 100 μM putrescine added. After 6 days, cells were washed and labeled with pHrodo Red AM dye. IncuCyte analysis was then performed to monitor intracellular acidity over time. After 2 hours of measurement, nigericin/valinomycin was added. *n* = 4 wells per group, representative of three independent experiments. (A) *n* = 4 control and tumor-bearing brains/spleens were analyzed. (B to D) *n* = 3 per group, representative of two independent experiments. Significance was calculated via unpaired Student's *t* tests (A and D) and one-way ANOVA with Tukey's post hoc for individual comparisons in (C) and (F): \**P* < 0.05, \*\**P* < 0.01, and \*\*\**P* < 0.001.



This occurs because proton/CO<sub>2</sub> extrusion is needed to maintain intracellular pH during glycolysis (36–38). This has been recently shown as a method by which T cells hinder their own effector functions (39). As tumors tend to use extensive glycolytic metabolism, this may be why atypical proton extruders carbonic anhydrases IX and XII are up-regulated in solid tumors (40, 41). Therefore, it is possible that polyamines are generated within TAMCs to facilitate intracellular pH normalization and, thus, glycolytic metabolism.

To test this, we generated TAMCs with or without DFMO in vitro, cultured the cells under decreasing pHs, and performed extracellular flux analysis using Seahorse analysis (Fig. 6A). Under all conditions of reducing pH, both control and DFMO pretreated samples had a significant reduction in ECAR (extracellular acidification rate) ( $P < 0.001$  for all comparisons within groups at each pH). When comparing across treatments, basal ECAR was reduced in DFMO-treated TAMCs under all pHs (pH 7.4:  $69.1 \pm 2$  mpH/min in control versus  $35.0 \pm 3.7$  mpH/min in DFMO pretreated; pH 7.0:  $51.0 \pm 1$  mpH/min in control versus  $26.0 \pm 0.8$  mpH/min in DFMO pretreated; pH 6.7:  $30.6 \pm 0.7$  mpH/min in control versus  $20.0 \pm 1.3$  mpH/min in DFMO pretreated;  $P < 0.001$ ). Furthermore, both glucose-stimulated ECAR and maximal ECAR were significantly reduced by DFMO pretreatment at pH 7.4 and 7.0 ( $P < 0.001$ ). At pH 6.7, differences between DFMO and control groups were not observed, suggesting a limitation to the buffering capacity of polyamines in this system.

Last, to determine whether metabolic perturbation of TAMCs occurs in the context of glioma, we performed TAMC isolation and performed <sup>13</sup>C-glucose flux analysis from CT-2A tumor-bearing animals (Fig. 6B). DFMO-pretreated animals had significantly reduced glycolytic metabolism as shown by reduced M+3 pyruvate ( $44.6 \pm 3.8\%$  in control versus  $10.2 \pm 4.6\%$  in DFMO treated;  $P < 0.01$ ) and lactate incorporation ( $1.9 \pm 0.2\%$  in control versus  $1.0 \pm 0.13\%$  in DFMO treated;  $P < 0.05$ ). Using an in vivo carbon flux model (42), we assessed <sup>13</sup>C-glucose flux in vivo in control and DFMO-treated animals to look at bulk tumor <sup>13</sup>C-glucose flux (Fig. 6C). While there was enhanced M+3 lactate incorporation by the bulk TME compared to the liver ( $52.5 \pm 2.3\%$  in tumor versus  $20.7 \pm 3.2\%$  in the liver;  $P < 0.01$ ), there was no change in the bulk tumor glycolytic metabolism of DFMO-treated animals. This final observation highlights the specificity of DFMO on blunting TAMC immunosuppression in GBM.

## DISCUSSION

Arginase-1 expression has been considered a hallmark of the suppressive myeloid phenotype for the past 20 years (43, 44). Alongside these observations, many studies have shown that the catabolism of the arginase-1 metabolite, ornithine (via ODC1), broadly promotes the immunosuppression of myeloid lineage cells (29, 45, 46). Supporting the importance of polyamine generation in myeloid function, a recent critical study revealed that macrophages generate polyamines to support the alternative activation of macrophages via the hypusination of EIF5 $\alpha$  (47). While there is abundant evidence that this pathway is important for myeloid cell to induce immunosuppression, the mechanism why this metabolic pathway is invoked has yet to be understood. Our results provide a potential metabolic explanation whereby the generation of the polyamine putrescine acts as pH buffer against hostile acidic TME to promote both the survival and metabolic functions of TAMCs in GBM.

Immunosuppressive or “inflammation-resolving” myeloid cells must enter an inflamed tissue to exert their effects. Both tumor

tissues and inflamed tissues are hypoxic (48) and, by extension, acidic (49, 50). The ability of cells to function or survive under such intense environmental stress likely underlies their ability to halt an ongoing immune response. This appears to be particularly important in the context of glioma, as we identified via unbiased methods that arginine metabolism is a central metabolic tenet of TAMCs in GBM. This comports with a seminal study on the function of arginase-1 myeloid-driven immunosuppression in cancer (51). We found that not only was the arginase-1 pathway involved in the generation of ornithine in TAMCs but so was the de novo creatine pathway [via Glycine amidinotransferase (GATM)], which also generates ornithine. Our results also highlighted that the fate of arginine in TAMCs is directed toward polyamine generation and not the iNOS pathway, although myeloid cells are known to use this pathway for immunosuppression in other malignancies (52). One potential explanation is the preponderance of M-MDSCs in both human and murine models of glioma (9, 53). As PMN-MDSCs are recognized as the major producer of iNOS-mediated immunosuppression (54), it may be particularly relevant to look at myeloid-polyamine metabolism in the context of GBM. Why the metabolic phenotype of TAMCs differs so markedly from peripheral myeloid cells is likely a result of predominate migration and accumulation of MDSC in gliomas (53), intratumoral proliferation of myeloid cells (55), or cues that come from the TME (56). How these cues influence metabolic phenotypes is unknown and an important topic for future exploration. While this study was focused mainly on TAMCs, microglial populations were also affected by DFMO administration, suggesting that microglia may also play a role in the inflammatory responses to polyamine blockade.

Our second observation is that the polyamine metabolic pathway is critical for TAMC-mediated immunosuppression in GBM. The importance of polyamine anabolism on TAMC function is consistent with the aforementioned studies on the importance of the polyamine pathway in the maintenance of M2 myeloid lineage cells. The mechanistic insights into these observations were mainly attributed to changes in gene expression (29) or epigenetic status of the cells (45, 46). We did find that DFMO might exert its role by up-regulating TNF $\alpha$ , a proinflammatory cytokine seen up-regulated in ODC conditional KO mice (45). Further work is needed to understand how polyamine influences inflammatory gene expression.

Our third observation is that blockade of de novo polyamine generation via DFMO is therapeutically relevant for murine models of GBM. It is unexpected that monotherapy with DFMO caused increased animal survival in immunocompetent animals, which was abrogated in the immunodeficient model of the disease (57). As our data showed that significant survival benefit with DFMO was abrogated in RAG-1 KO mice, this indicates that DFMO functions via promotion of antitumor adaptive immune responses. This result highlights the importance of the de novo polyamine pathway on immunity that is compartmental in nature. The immunologic consequences of polyamine inhibition are still relatively unknown, but our work shows that myeloid cells are likely the primary target of such therapy. We saw that treatment with DFMO increased PD-L1 expression in the TME, which has been recently used as an indicator of increased inflammation in glioma (58). For this reason, we believe that targeting the PD–PD-L1 pathway will further enhance adaptive immune response by blocking T cell exhaustion (59). We found that polyamine inhibition can work in concert with T cell-based immunotherapies for this disease. The mechanisms behind this combinatorial approach are currently under investigation.

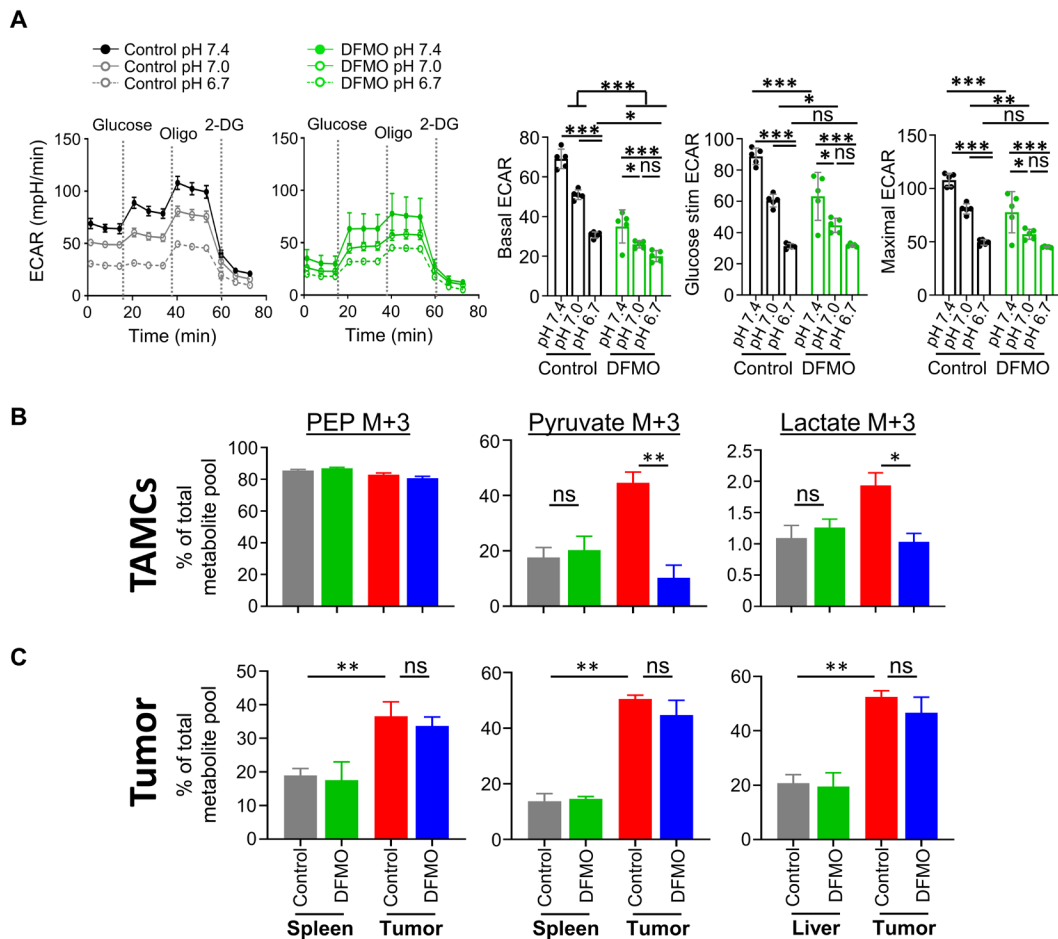


**Fig. 6. Polyamines promote the metabolism of TAMCs under conditions of pHe.** (A) TAMCs were generated in the context of DFMO, and after 6 days of differentiation, cells were lifted, adhered using Cell-Tak adhesive, and cultured in decreasing pH medium. Immediately following addition of acidic medium, Seahorse extracellular flux analysis was performed to determine glycolytic metabolism. (B) DFMO-treated animals had TAMCs isolated, and ex vivo  $^{13}\text{C}$ -glucose flux was performed. (C) In vivo  $^{13}\text{C}$ -glucose flux was performed by infusion of  $^{13}\text{C}$ -glucose (100 mg/ml) over a 2.5-hour period. After infusion, tumor, adjacent parenchyma, and liver were flash-frozen for bulk metabolite analysis. (A)  $n = 5$  per group, representative of two independent experiments. (B) Each sample is  $n = 10$  mice pooled per sample, with three pooled samples submitted in triplicate; data are representative of two independent experiments. (C)  $n = 3$  mice were individually analyzed per group. Statistics were calculated via unpaired Student's  $t$  tests: \* $P < 0.05$ , \*\* $P < 0.01$ , and \*\*\* $P < 0.001$ . 2-DG, 2-deoxyglucose; PEP, phosphoenolpyruvate.

Unfortunately, polyamine inhibition has not yet yielded significant benefits in the clinic (60). This is similar to clinical experience with immunotherapies (61), and the reasons for this are currently unknown. Recent work has shown that steroid administration and standard-of-care therapies, both of which are frequently given to patients, can potentially inhibit antitumor immune responses (62, 63) and may play a role in treatment resistance, but more work is needed to understand these interactions.

A caveat of these treatment modalities is that they did not elicit long-term survival benefit. The reasons for this are unknown, but considering that T cells undergo significant metabolic programming at different stages of activation/memory (64), it is possible that de novo polyamine generation is important for an immunological memory phenotype or some other unknown processes critical for long-term antitumor immunity. In the future, it will be critical to uncover when polyamine generation is needed for T cells and why. Related to this point is that polyamines can be acquired exogenously. The ability of cells to complement de novo polyamine generation

with exogenous uptake has inspired compounds that inhibit polyamine uptake (65). There are currently a number of clinical trials focused on this combinatorial modality. As the uptake inhibitors have very limited accessibility to the CNS, future work will be focused on understanding whether we can deliver this next-generation polyamine therapeutics to patients with GBM.

Our last observation is that polyamines act as an intracellular pH buffer that promotes both the survival and metabolic functions of TAMCs in GBM. Polyamines are incredibly basic compounds, which were initially discovered as the major constituent of semen (66). This acidic environment is recapitulated in solid tumors, and our data show that TAMCs generate their own basic metabolites to survive under these harsh conditions. This phenomenon is not without precedent, as a previous study showed that polyamine blockade induces intracellular acidification in leukemic cells (67). Many tumors are known to up-regulate polyamine generation, which is why studies have argued that polyamines are immunosuppressive compounds (65, 68). Our data, however, suggest that the presence of polyamines

is actually a survival mechanism for cells. Perhaps endowing T cells with an enhanced ability to generate their own polyamines may actually be beneficial for their function in tumors. As both glycolytic and mitochondrial metabolism generate a large amount of acidic end products, we have also observed that de novo polyamine generation also maintains intracellular pH and, thus, metabolic fitness of TAMCs. Note that whole-tumor glucose flux did not reveal the same changes induced by DFMO treatment on TAMCs, further highlighting the specificity of the de novo polyamine pathway on this immunosuppressive subset.

In summation, this work shows that polyamine metabolism is a central tenet of immunosuppression in GBM that can be targeted effectively. This lays groundwork for future studies to understand the exact roles that polyamines have on different glioma-infiltrating cellular subsets and how we can use them to promote antitumor immunity for this untreatable disease.

## MATERIALS AND METHODS

### Mouse models

All mice were housed at the Center for Comparative Medicine at Northwestern Feinberg School of Medicine. Mice are all housed in a conventional barrier facility with 12-hour light/12-hour dark cycles and ad libitum access to food and water. C57/Bl6, OT-1 Bl6, and RAG<sup>0/0</sup> Bl6 mice were obtained from The Jackson Laboratory (Bar Harbor, ME) and bred for use in experiments. All experiments were performed in mice 6 to 8 weeks old, age- and gender-matched. Equal numbers of male and female mice were used whenever possible. For all Kaplan-Meier curves, C57/Bl6 mice were purchased at 6 weeks old, and numbers of male/female mice were always equivalent between control and experimental groups. All mouse protocols performed in this study were approved by Northwestern's Institutional Animal Care and Use Committee under study approval number IS00002459.

### Cell lines and tumor implantation

The CT-2A tumor line was initially obtained from T. Seyfried (Boston College). The GL-261 tumor line was purchased from the National Cancer Institute (NCI). Cells were cultured in Dulbecco's modified Eagle's medium (Corning) supplemented with 10% fetal bovine serum (FBS; HyClone) and penicillin-streptomycin. For injections, cells were lifted with trypsin-EDTA (Corning), washed with phosphate-buffered saline (PBS), and suspended at a concentration of  $7.5 \times 10^4$  cells ( $1.0 \times 10^5$  for GL-26 and  $2 \times 10^5$  for GL-26-OVA) per 2.5  $\mu$ l. Mice were implanted with CT-2A using a stereotactic apparatus following the exact specifications as described previously (69). Following this method, tumor cell injection has a 100% engraftment rate in C57/Bl6 mice. GL-261 lines overexpressing OVA were generated previously (70) and cultured in G-418 (200  $\mu$ g/ml; Sigma-Aldrich) to maintain selection pressure.

### Tissue and cellular isolations

#### Mice

Tumor-bearing mice were perfused with 1 $\times$  PBS before tumors were removed and homogenized in Hanks' balanced salt solution (Gibco, Thermo Fisher Scientific) using a Dounce homogenizer (Sigma-Aldrich). Homogenized tissues were passed through a 70- $\mu$ m filter, spun, and then resuspended in 30% Percoll (GE Healthcare) layered carefully over 70% Percoll solution for density gradient centrifuga-

tion as performed previously (69). Interface was collected and washed in PBS before any downstream analysis. For splenic isolation, spleens were directly homogenized through a 70- $\mu$ m strainer, followed by red blood lysis using ACK buffer (Gibco, Thermo Fisher Scientific). Cells were washed and then used for all downstream analysis.

#### Humans

Fresh tumor tissue was harvested from newly diagnosed GBM patients, manually diced with a sterile scalpel, and incubated with collagenase/deoxyribonuclease 1 (DNase 1)/Tosyl-L-lysyl-chloromethane hydrochloride (TLCK) (all Sigma-Aldrich) mixture for 15-min intervals at 37°C. Once tissue was digested, it was homogenized and leukocytes were isolated via Percoll gradient centrifugation as described for mouse tumor isolation. For peripheral blood mononuclear cell (PBMC) isolation, blood was isolated from matched patients and leukocytes were isolated via Ficoll-Paque® PLUS (GE Healthcare) density gradient centrifugation. PBMCs were washed and used for all downstream analysis.

### Magnetic bead isolation of cells

To isolate specific populations of cells, single-cell suspensions as isolated above are preblocked with anti-CD16/32 for 15 min at 4°C. We then used the biotinylated anti-Gr1 (clone RB6-8C5), anti-CD8 $\beta$ , or anti-CD163 antibodies (all from Thermo Fisher Scientific) to label murine myeloid, CD8<sup>+</sup>, and human monocytes, respectively. Next, the cells were washed and then incubated with anti-biotin magnetic beads (Miltenyi Biotec) before performing manual positive selection using MS columns (Miltenyi Biotec). Purified cells were analyzed for all downstream metabolic analyses.

### In vitro T cell/TAMC generation

TAMCs were generated as described previously (9). Briefly, bone marrow precursors were isolated from the femurs of C57/Bl6 mice or C57 OT-1 mice and resuspended in RPMI supplemented with recombinant granulocyte-macrophage colony-stimulating factor (GM-CSF) (40 ng/ml) and 50% of 0.2- $\mu$ m sterile-filtered CT-2A supernatant. After 3 days, cells were washed and replaced with the same medium. At 6 days, cells were validated to be phenotypically similar to TAMCS in vivo (9). CD8<sup>+</sup> T cells were isolated from the spleens of mice using a MagniSort CD8+ T cell Enrichment kit (Thermo Fisher Scientific) and stimulated with mouse T cell-activating Dynabeads (Thermo Fisher Scientific). For antigen-specific activation, we used SIINFEKL peptide (50 ng/ml) on OT-1 isolated T cells.

### Histological evaluation of tumors

For hematoxylin and eosin (H&E) analysis, tumors were implanted, and 5 days after tumor implantation, brains were harvested and fixed overnight in 10% neutral buffered formalin overnight. Samples were submitted to the Northwestern Pathology Core, where paraffin embedding and H&E staining were performed. Validation of tumor engraftment was performed by certified neuropathologist. For immunofluorescence, mice were perfused with 10 ml of PBS, and brains were snap-frozen in OCT (Sakura Tissue-Tek). Brains were then cut into 8- $\mu$ m-thick sections using a CM1860 cryostat (Leica, Wetzlar, Germany). Sections were fixed with 100% methanol pre-chilled at -80°C for 10 min. Sections were blocked in 5% normal rat serum for 30 min, washed, and then incubated 1:100 with anti-CD8-PE (phycoerythrin) and anti-CD11b-Alexa Fluor 488. Last, sections were mounted using Fluoroshield with DAPI (4',6-diamidino-2-phenylindole) (Sigma-Aldrich). Four control and four DFMO-treated mice were used for analysis, with two independent images

analyzed for infiltration per mouse. Image identities were blinded and counted blindly by A.R.

### Immunophenotyping

Single-cell suspensions were blocked with anti-CD16/32 antibodies before incubation with antibody panels as described below. For cytokine staining, cells were preincubated with phorbol 12-myristate 13-acetate (PMA)/ionomycin + brefeldin A for 4 hours before fixation and intracellular staining. The Foxp3 fixation/permeabilization (Invitrogen, Thermo Fisher Scientific) protocol was used for all intracellular flow cytometric analysis (71).

The following myeloid panel was used for flow cytometric analysis: Live/Dead eFluor 780 (Thermo Fisher Scientific), anti-CD45 BV510, anti-CD3 PE-Cy7, anti-C11b Pacific Blue, anti-Ly6C AF 700, anti-Ly6G peridinin chlorophyll protein (Percp)-cy5.5, anti-arginase 1 allophycocyanin (APC), anti-PD-L1 PE, anti-CD11c BV605, anti-TGF- $\beta$ -LAP BV711, and anti-interleukin-10 (IL-10) fluorescein isothiocyanate (FITC). All antibodies are purchased from BioLegend except arginase-1 (Thermo Fisher Scientific).

The following flow cytometry panel was used for lymphocytic analysis: Live/Dead eFluor 780, anti-CD45 BV510, anti-CD4 PE-Cy7, anti-CD8-BV605, anti-CD44 Percpcy5.5, anti-Foxp3 eFluor 450, anti-CD19 BV711, anti-CD25 PE, anti-interferon  $\gamma$  (IFN $\gamma$ ) AF 700, anti-TNF $\alpha$  FITC, and anti-granzyme B Alexa Fluor 647. All antibodies are purchased from BioLegend except Foxp3 (Thermo Fisher Scientific). This allows us to define conventional T cells (CD45<sup>+</sup>CD3<sup>+</sup>CD4<sup>+</sup>CD8<sup>-</sup>Foxp3<sup>-</sup>), regulatory T cells (CD45<sup>+</sup>CD3<sup>+</sup>CD4<sup>+</sup>CD8<sup>-</sup>Foxp3<sup>+</sup>CD25<sup>+</sup>), B cells (CD45<sup>+</sup>CD3<sup>-</sup>CD19<sup>+</sup>), and natural killer (NK) cells (CD45<sup>+</sup>CD3<sup>-</sup>NK1.1<sup>+</sup>). IFN $\gamma$ , TNF $\alpha$ , and granzyme B expression are a measure of inflammatory phenotype on each of these cells.

The following flow cytometry panel was used for tetramer analysis: Live/Dead eFluor 780, anti-CD45 BV510, anti-CD4 PE-Cy7, anti-CD8 PE (clone KT15 from Medical & Biological Laboratories Co.), anti-CD44 Percpcy5.5, anti-Foxp3 eFluor 450, anti-CD11b BV711, and anti-SIINFEKL-H2<sup>kb</sup> tetramer Alexa Fluor 488. The conjugated tetramers were generated by the National Institutes of Health (NIH) Tetramer Facility at Emory University. Tetramer staining was performed at room temperature for 45 min.

For pHrodo Red intracellular pH measurement, cells from spleen or tumor were counted, normalized, and incubated with 500 nm pHrodo Red dye in PBS at 37°C for 30 min before being washed twice with 2% FBS/PBS wash buffer. This step was performed before live/dead and antibody staining as described above.

For cell necrosis/apoptotic measurement, TAMCs were washed with PBS before being incubated with live/dead eFluor 780 for 30 min on ice. Cells were washed twice with annexin V binding buffer (BioLegend) before being incubated with annexin V FITC (1:20; BioLegend) for 15 min at room temperature. Cells were then washed twice with annexin binding buffer (Becton Dickinson) and kept in binding buffer during flow cytometric analysis.

### Extracellular flux assays

Extracellular flux analysis on TAMCs was performed using a Seahorse XFe96 analyzer (Agilent), as previously described (72). Briefly, TAMCS were lifted and adhered to microplates using Cell-Tak Adhesive (Thermo Fisher Scientific) at a density of  $1 \times 10^5$  cells per well. Glycolytic flux was measured using the glycolysis stress test (Agilent) following the manufacturer's guidelines.

### RNA-seq analysis

Fourteen days after CT-2A tumor implantation, 10 mice were pooled for each  $n$  reported in this study, followed by Gr1 magnetic bead isolation, and RNA was isolated using TRIzol (Thermo Fisher Scientific)-based RNA purification. Briefly, 0.2 ml of chloroform was added to TRIzol samples; top RNA-containing layer was precipitated with 70% isopropanol. Pellets were dried, then resuspended in sterile water, and sent for analysis. Isolated samples were sent to Novogene, which analyzed RNA for quality and provided all data as total counts and fpkm (fragments per kilobase per million reads) values. Fpkm values are reported throughout this manuscript.

### Metabolic flux analyses

#### Arginine flux

SILAC RPMI medium was supplemented with 10% dialyzed FBS (Fisher), glycine (40 mg/ml), and U<sup>13</sup>C-arginine (200 mg/ml; Cambridge Isotope Laboratories). All cells were washed with blank SILAC before being reconstituted in <sup>13</sup>C medium at a concentration of  $1 \times 10^6$  to  $2 \times 10^6$  cells/ml for 2 to 4 hours, depending on the assay. Cells were lifted and washed twice with PBS before pellets were flash-frozen and stored at  $-80^\circ\text{C}$  until metabolite extraction. Pellets were resuspended in 80% methanol/20% H<sub>2</sub>O and then lysed by 3 $\times$  cycles of heat shock (LN<sub>2</sub> freezing followed by 42°C water bath). Samples were then spun at 14,000 rpm for 15 min; supernatant was collected and analyzed as described below.

#### Glucose flux

Glucose-free RPMI medium was supplemented with 10% dialyzed FBS and U<sup>13</sup>C-glucose (2 g/liter; Cambridge Isotope Laboratories). All cells were washed with blank SILAC before being reconstituted in <sup>13</sup>C medium at a concentration of  $1 \times 10^6$  to  $2 \times 10^6$  cells/ml for 2 to 4 hours, depending on the assay. Cells were lifted and washed twice with PBS before pellets were flash-frozen and stored at  $-80^\circ\text{C}$  until metabolite extraction.

#### In vivo flux

In vivo glucose flux was performed exactly as described previously (42), adapted to our tumor models. Two weeks after tumor implantation (7 days after DFMO administration), mice were continuously anesthetized with isoflurane using an anesthetic vaporizer (Harvard Apparatus) connected to mouse tail illuminator/restrainer (Braintree Scientific). U<sup>13</sup>C-Glucose was diluted to 100 mg/ml in 0.9% saline (Baxter) and loaded into 1-ml Luer-lock syringes (Becton Dickinson). Loaded tubes were connected via MicroRenathane tubing (Braintree) to a 27-gauge scalp-vein butterfly needle (Exelint International). Mice were injected with a 130- $\mu\text{l}$  bolus of label, before being infused at a rate of 2.5  $\mu\text{l}/\text{min}$  using a syringe pump (Braintree) for 2.5 hours. After infusion, mice were immediately euthanized and tumor, normal brain, and liver were flash-frozen in LN<sub>2</sub> and stored at  $-80^\circ\text{C}$  until extraction. For metabolite extraction, 50 mg of frozen tissue was homogenized in 3 ml of 80% methanol/20% H<sub>2</sub>O using a Polytron homogenizer (Kinematica USA). Homogenized samples were incubated at  $-80^\circ\text{C}$  overnight and then spun at 14,000 rpm for 15 min; supernatant was collected and analyzed as described below.

#### Normalizations for metabolic data

To ensure rigor of data presented, two independent forms of normalization were performed on all samples. For samples that involved cellular isolation, we normalized each submission to the lowest cell count obtained to ensure uniformity in injection. These numbers of cells submitted to LC-MS/MS were always between  $5 \times 10^5$  and  $2 \times 10^6$  cells. For in vivo infusion data, we weighed tissues to



normalize them across samples (50 mg of tissue was uniformly used). The secondary method of normalization is to determine total ion count (TIC) and normalize all samples to the lowest TIC reading after the LC-MS/MS has been run. This is the gold standard method of normalization of MS data (73).

### Hydrophilic metabolite profiling

Isolated TAMC and CD8<sup>+</sup> T cells samples were dried using a SpeedVac. Acetonitrile (50%) was added to the tube for reconstitution following overtaxing for 30 s. Sample solution was then centrifuged for 15 min at 20,000g and 4°C. Supernatant was collected for LC-MS analysis. Samples were analyzed by high-performance LC (HPLC) and high-resolution MS and MS/MS (HPLC-MS/MS). The system consists of Thermo Q Exactive with an electrospray source and an UltiMate3000 (Thermo Fisher Scientific) series HPLC consisting of a binary pump, degasser, and autosampler outfitted with an XBridge Amide column (Waters; dimensions of 4.6 mm by 100 mm and a 3.5- $\mu$ m particle size). The mobile phase A contained 95% water/5% acetonitrile (v/v), 20 mM ammonium hydroxide, and 20 mM ammonium acetate (pH 9.0); phase B was 100% acetonitrile. The gradient was performed as follows: 0 min, 15% A; 2.5 min, 30% A; 7 min, 43% A; 16 min, 62% A; 16.1 to 18 min, 75% A; and 18 to 25 min, 15% A with a flow rate of 400  $\mu$ l/min. The capillary of the electrospray ionization source was set to 275°C, with sheath gas at 45 arbitrary units, auxiliary gas at 5 arbitrary units, and the spray voltage at 4.0 kV. In positive/negative polarity switching mode, a mass/charge ratio (*m/z*) scan range from 70 to 850 was chosen and MS1 data were collected at a resolution of 70,000. The automatic gain control target was set at  $1 \times 10^6$ , and the maximum injection time was 200 ms. The top five precursor ions were subsequently fragmented, in a data-dependent manner, using the higher-energy collisional dissociation cell set to 30% normalized collision energy in MS2 at a resolution power of 17,500. Data acquisition and analysis were carried out by Xcalibur 4.1 software and TraceFinder 4.1 software, respectively (both from Thermo Fisher Scientific).

### pHLIP dye measurement of pH

Mice were intracranially injected with CT-2A or saline. Fourteen days after tumor engraftment, 100  $\mu$ l of pHLIP-Cy5.5 dye at 100  $\mu$ M (synthesized and provided by Y.K.R.) was administered via intravenous injection. Twenty-four hours after injection, brains and spleens from both controls and tumor-bearing mice were immediately harvested and scanned with a spectral Lago (Spectral Imaging Systems, Tucson, AZ) with excitation at 675 nm and emission at 730 nm. The fluorescence intensities in regions of interest were calculated using Aura Imaging Software.

### IncuCyte time-based fluorescence assay

TAMCs were generated and treated with inhibitors DFMO as described above. At day 6, cells were labeled with pHrodo Red AM, and the same number of cells ( $1 \times 10^6$  cells) was labeled with the same concentration of dye before being washed for IncuCyte analysis. TAMCs were resuspended at a concentration of  $1 \times 10^5$ /ml in live cell imaging buffer (Thermo Fisher Scientific) at a pH of 7.4, 7.0, and 6.7. To generate a pH standard curve, TAMCs were pre-treated with pH 7.4, 7.0, and 6.7 solution containing nigericin/valinomycin to clamp intracellular pH to extracellular pH. The fluorescence measurement of these standards was used to generate a curve by which the experimental groups were measured. The membrane-

impermeant dye IncuCyte Cytotox Green (Essen Bioscience) was added at a 1:1000 dilution to monitor for apoptosis. Cells were imaged every 20 min for 4 hours, and fluorescence flux of pHrodo Red was measured over time. After 2 hours of measurement, nigericin/valinomycin was added to experimental wells to measure clamped pH.

### Statistical analysis

Statistical significance across two groups was determined using two-tailed unpaired Student's *t* test performed on figures with individual comparisons. One-way analysis of variance (ANOVA) with Tukey's post hoc was performed for comparisons of three or more groups. Kaplan-Meier curves were generated, and log-rank test was performed to determine significance of in vivo survival rates. *P* values were calculated in Prism software (GraphPad, San Diego, CA), and the significance is as stated in the figure legends. Error bars are shown as  $\pm$ SEMs for all figures. For pHrodo Red analyses, mixed-effects models for longitudinal data were performed and post hoc analysis was performed in both R and SAS, which produced similar results. For MetaboAnalyst data, normalized peak areas were inputted into online software, and heatmaps were generated based on *t* test statistical significance. MetaboAnalyst figure was automatically generated by the MetaboAnalyst website (74). All statistics were validated by T.X.

### SUPPLEMENTARY MATERIALS

Supplementary material for this article is available at <http://advances.sciencemag.org/cgi/content/full/7/8/eabc8929/DC1>

### REFERENCES AND NOTES

1. R. Stupp, W. P. Mason, M. J. van den Bent, M. Weller, B. Fisher, M. J. B. Taphoorn, K. Belanger, A. A. Brandes, C. Marosi, U. Bogdahn, J. Curschmann, R. C. Janzer, S. K. Ludwin, T. Gorlia, A. Allgeier, D. Lacombe, J. G. Cairncross, E. Eisenhauer, R. O. Mirimanoff; European Organisation for Research and Treatment of Cancer Brain Tumor and Radiotherapy Groups; National Cancer Institute of Canada Clinical Trials Group, Radiotherapy plus concomitant and adjuvant temozolomide for glioblastoma. *N. Engl. J. Med.* **352**, 987–996 (2005).
2. R. Stupp, S. Taillibert, A. A. Kanner, S. Kesari, D. M. Steinberg, S. A. Toms, L. P. Taylor, F. Lieberman, A. Silvani, K. L. Fink, G. H. Barnett, J.-J. Zhu, J. W. Henson, H. H. Engelhard, T. C. Chen, D. D. Tran, J. Sroubek, N. D. Tran, A. F. Hottinger, J. Landolfi, R. Desai, M. Caroli, Y. Kew, J. Honnorat, A. Idbaih, E. D. Kirson, U. Weinberg, Y. Palti, M. E. Hegi, Z. Ram, Maintenance therapy with tumor-treating fields plus temozolomide vs temozolomide alone for glioblastoma: A randomized clinical trial. *JAMA* **314**, 2535–2543 (2015).
3. W. Tomaszewski, L. Sanchez-Perez, T. F. Gajewski, J. H. Sampson, Brain tumor microenvironment and host state: Implications for immunotherapy. *Clin. Cancer Res.* **25**, 4202–4210 (2019).
4. V. Thorsson, D. L. Gibbs, S. D. Brown, D. Wolf, D. S. Bortone, T.-H. O. Yang, E. Porta-Pardo, G. F. Gao, C. L. Plaisier, J. A. Eddy, E. Ziv, A. C. Culhane, E. O. Paull, I. K. A. Sivakumar, A. J. Gentles, R. Malhotra, F. Farshidfar, A. Colaprico, J. S. Parker, L. E. Mose, N. S. Vo, J. Liu, Y. Liu, J. Rader, V. Dhankani, S. M. Reynolds, R. Bowlby, A. Califano, A. D. Cherniack, D. Anastassiou, D. Bedognetti, Y. Mokrab, A. M. Newman, A. Rao, K. Chen, A. Krasnitz, H. Hu, T. M. Malta, H. Noushmeh, C. S. Pedamallu, S. Bullman, A. I. Ojesina, A. Lamb, W. Zhou, H. Shen, T. K. Choueiri, J. N. Weinstein, J. Guinney, J. Saltz, R. A. Holt, C. S. Rabkin; Cancer Genome Atlas Research Network, A. J. Lazar, J. S. Serody, E. G. Demicco, M. L. Disis, B. G. Vincent, I. Shmulevich, The immune landscape of cancer. *Immunity* **48**, 812–830.e14 (2018).
5. N. Kamran, P. Kadiyala, M. Saxena, M. Candolfi, Y. Li, M. A. Moreno-Ayala, N. Raja, D. Shah, P. R. Lowenstein, M. G. Castro, Immunosuppressive myeloid cells' blockade in the glioma microenvironment enhances the efficacy of immune-stimulatory gene therapy. *Mol. Ther.* **25**, 232–248 (2017).
6. J. P. Antonios, H. Soto, R. G. Everson, D. Moughon, J. R. Orpilla, N. P. Shin, S. Sedighim, J. Tregler, S. Odesa, A. Tucker, W. H. Yong, G. Li, T. F. Cloughesy, L. M. Liaw, R. M. Prins, Immunosuppressive tumor-infiltrating myeloid cells mediate adaptive immune resistance via a PD-1/PD-L1 mechanism in glioblastoma. *Neuro Oncol.* **19**, 796–807 (2017).
7. J. Yuan, H. M. Levitin, V. Frattini, E. C. Bush, D. M. Boyett, J. Samanamud, M. Ceccarelli, A. Dovas, G. Zanazzi, P. Canoll, J. N. Bruce, A. Lasorella, A. Iavarone, P. A. Sims, Single-cell



- transcriptome analysis of lineage diversity in high-grade glioma. *Genome Med.* **10**, 57 (2018).
8. T. J. Alban, A. G. Alvarado, M. D. Sorensen, D. Bayik, J. Volovetz, E. Serbinowski, E. E. Mulkearns-Hubert, M. Sinyuk, J. S. Hale, G. R. Onzi, M. M. Graw, P. Huang, M. M. Grabowski, C. A. Wathen, M. S. Ahluwalia, T. Radivoyevitch, H. I. Kornblum, B. W. Kristensen, M. A. Vogelbaum, J. D. Lathia, Global immune fingerprinting in glioblastoma patient peripheral blood reveals immune-suppression signatures associated with prognosis. *JCI Insight* **3**, e122264 (2018).
  9. P. Zhang, J. Miska, C. Lee-Chang, A. Rashidi, W. K. Panek, S. An, M. Zannikou, A. Lopez-Rosas, Y. Han, T. Xiao, K. C. Pituch, D. Kanojia, I. V. Balyasnikova, M. S. Lesniak, Therapeutic targeting of tumor-associated myeloid cells synergizes with radiation therapy for glioblastoma. *Proc. Natl. Acad. Sci. U.S.A.* **116**, 23714–23723 (2019).
  10. C. Lee, H. Jeong, Y. Bae, K. Shin, S. Kang, H. Kim, J. Oh, H. Bae, Targeting of M2-like tumor-associated macrophages with a melittin-based pro-apoptotic peptide. *J. Immunother. Cancer* **7**, 147 (2019).
  11. S. M. Pyonteck, L. Akkari, A. J. Schuhmacher, R. L. Bowman, L. Sevenich, D. F. Quail, O. C. Olson, M. L. Quick, J. T. Huse, V. Teijeiro, M. Setty, C. S. Leslie, Y. Oei, A. Pedraza, J. Zhang, C. W. Brennan, J. C. Sutton, E. C. Holland, D. Daniel, J. A. Joyce, CSF-1R inhibition alters macrophage polarization and blocks glioma progression. *Nat. Med.* **19**, 1264–1272 (2013).
  12. R. D. Leone, L. Zhao, J. M. Englert, I.-M. Sun, M.-H. Oh, I.-H. Sun, M. L. Arwood, I. A. Bettencourt, C. H. Patel, J. Wen, A. Tam, R. L. Blosser, E. Prchalova, J. Alt, R. Rais, B. S. Slusher, J. D. Powell, Glutamine blockade induces divergent metabolic programs to overcome tumor immune evasion. *Science* **366**, 1013–1021 (2019).
  13. M. O. Johnson, M. M. Wolf, M. Z. Madden, G. Andrejeva, A. Sugiura, D. C. Contreras, D. Maseda, M. V. Liberti, K. Paz, R. J. Kishnot, M. E. Johnson, A. A. de Cubas, P. Wu, G. Li, Y. Zhang, D. C. Newcomb, A. D. Wells, N. P. Restifo, W. K. Rathmell, J. W. Locasale, M. L. Davila, B. R. Blazar, J. C. Rathmell, Distinct regulation of Th17 and Th1 cell differentiation by glutaminase-dependent metabolism. *Cell* **175**, 1780–1795.e19 (2018).
  14. M. Harel, R. Ortenberg, S. K. Varanasi, K. C. Mangalaha, M. Mardamshina, E. Markovits, E. N. Baruch, V. Tripple, M. Arama-Chayoth, E. Greenberg, A. Shenoy, R. Ayasun, N. Knafo, S. Xu, L. Anafi, G. Yanovich-Arad, G. D. Barnabas, S. Ashkenazi, M. J. Besser, J. Schachter, M. Bosenberg, G. S. Shadel, I. Barshack, S. M. Kaech, G. Markel, T. Geiger, Proteomics of melanoma response to immunotherapy reveals mitochondrial dependence. *Cell* **179**, 236–250.e18 (2019).
  15. A. Mayer, F. Schneider, P. Vaupel, C. Sommer, H. Schmidberger, Differential expression of HIF-1 in glioblastoma multiforme and anaplastic astrocytoma. *Int. J. Oncol.* **41**, 1260–1270 (2012).
  16. D. Coman, Y. Huang, J. U. Rao, H. M. de Feyter, D. L. Rothman, C. Juchem, F. Hyder, Imaging the intratumoral-peritumoral extracellular pH gradient of gliomas. *NMR Biomed.* **29**, 309–319 (2016).
  17. S. Peppicelli, F. Bianchini, L. Calorini, Extracellular acidity, a “reappreciated” trait of tumor environment driving malignancy: Perspectives in diagnosis and therapy. *Cancer Metastasis Rev.* **33**, 823–832 (2014).
  18. A. Honasoge, H. Sontheimer, Involvement of tumor acidification in brain cancer pathophysiology. *Front. Physiol.* **4**, 316 (2013).
  19. A. Rashidi, J. Miska, C. Lee-Chang, D. Kanojia, W. K. Panek, A. Lopez-Rosas, P. Zhang, Y. Han, T. Xiao, K. C. Pituch, J. W. Kim, M. Talebian, J. Fares, M. S. Lesniak, GCN2 is essential for CD8<sup>+</sup> T cell survival and function in murine models of malignant glioma. *Cancer Immunol. Immunother.* **69**, 81–94 (2020).
  20. R. Mirzaei, S. Sarkar, V. W. Yong, T cell exhaustion in glioblastoma: Intricacies of immune checkpoints. *Trends Immunol.* **38**, 104–115 (2017).
  21. S. M. Evans, K. D. Judy, I. Dunphy, W. T. Jenkins, W.-T. Hwang, P. T. Nelson, R. A. Lustig, K. Jenkins, D. P. Magarelli, S. M. Hahn, R. A. Collins, M. S. Grady, C. J. Koch, Hypoxia is important in the biology and aggression of human glial brain tumors. *Clin. Cancer Res.* **10**, 8177–8184 (2004).
  22. C. A. Corzo, T. Condamine, L. Lu, M. J. Cotter, J. I. Youn, P. Cheng, H. I. Cho, E. Celis, D. G. Quiceno, T. Padhya, T. V. McCaffrey, J. C. McCaffrey, D. I. Gabrilovich, HIF-1 $\alpha$  regulates function and differentiation of myeloid-derived suppressor cells in the tumor microenvironment. *J. Exp. Med.* **207**, 2439–2453 (2010).
  23. A. L. Doedens, C. Stockmann, M. P. Rubinstein, D. Liao, N. Zhang, D. G. De Nardo, L. M. Coussens, M. Karin, A. W. Goldrath, R. S. Johnson, Macrophage expression of hypoxia-inducible factor-1 $\alpha$  suppresses T-cell function and promotes tumor progression. *Cancer Res.* **70**, 7465–7475 (2010).
  24. A. Calcinotto, P. Filipazzi, M. Groni, M. Iero, A. De Mitto, A. Ricupito, A. Cova, R. Canese, E. Jachetti, M. Rossetti, V. Huber, G. Parmiani, L. Generoso, M. Santinami, M. Borghi, S. Fais, M. Bellone, L. Rivoltini, Modulation of microenvironment acidity reverses anergy in human and murine tumor-infiltrating T lymphocytes. *Cancer Res.* **72**, 2746–2756 (2012).
  25. S. Pilon-Thomas, K. N. Kodumudi, A. E. El-Kenawi, S. Russell, A. M. Weber, K. Luddy, M. Damaghi, J. W. Wojtkowiak, J. J. Mulé, A. Ibrahim-Hashim, R. J. Gillies, Neutralization of tumor acidity improves antitumor responses to immunotherapy. *Cancer Res.* **76**, 1381–1390 (2016).
  26. T. Bohn, S. Rapp, N. Luther, M. Klein, T.-J. Bruehl, N. Kojima, P. A. Lopez, J. Hahlbrock, S. Muth, S. Endo, S. Pektor, A. Brand, K. Renner, V. Popp, K. Gerlach, D. Vogel, C. Lueckel, D. Arnold-Schild, J. Pouyssegur, M. Kreutz, M. Huber, J. Koenig, B. Weigmann, H.-C. Probst, E. von Stebut, C. Becker, H. Schild, E. Schmitt, T. Bopp, Tumor immunoevasion via acidosis-dependent induction of regulatory tumor-associated macrophages. *Nat. Immunol.* **19**, 1319–1329 (2018).
  27. T. R. Sippel, J. White, K. Nag, V. Tsvankin, M. Klaassen, B. K. Kleinschmidt-DeMasters, A. Waziri, Neutrophil degranulation and immunosuppression in patients with GBM: Restoration of cellular immune function by targeting arginase I. *Clin. Cancer Res.* **17**, 6992–7002 (2011).
  28. G. Kohanbash, K. McKaveney, M. Sakaki, R. Ueda, A. H. Mintz, N. Amankulor, M. Fujita, J. R. Ohlfest, H. Okada, GM-CSF promotes the immunosuppressive activity of glioma-infiltrating myeloid cells through interleukin-4 receptor- $\alpha$ . *Cancer Res.* **73**, 6413–6423 (2013).
  29. C. Ye, Z. Geng, D. Dominguez, S. Chen, J. Fan, L. Qin, A. Long, Y. Zhang, T. M. Kuzel, B. Zhang, Targeting ornithine decarboxylase by  $\alpha$ -difluoromethylornithine inhibits tumor growth by impairing myeloid-derived suppressor cells. *J. Immunol.* **196**, 915–923 (2016).
  30. V. A. Levin, S. E. Ictech, K. R. Hess, Clinical importance of eflornithine ( $\alpha$ -difluoromethylornithine) for the treatment of malignant gliomas. *CNS Oncol.* **7**, CNS16 (2018).
  31. S. Mandal, A. Mandal, H. E. Johansson, A. V. Orjalo, M. H. Park, Depletion of cellular polyamines, spermidine and spermine, causes a total arrest in translation and growth in mammalian cells. *Proc. Natl. Acad. Sci. U.S.A.* **110**, 2169–2174 (2013).
  32. A. Brett-Morris, B. M. Wright, Y. Seo, V. Pasupuleti, J. Zhang, J. Lu, R. Spina, E. E. Bar, M. Gajrati, R. Schur, Z.-R. Lu, S. M. Welford, The polyamine catabolic enzyme SAT1 modulates tumorigenesis and radiation response in GBM. *Cancer Res.* **74**, 6925–6934 (2014).
  33. A. K. Handa, T. Fatima, A. K. Mattoo, Polyamines: Bio-molecules with diverse functions in plant and human health and disease. *Front. Chem.* **6**, 10 (2018).
  34. M. Anderson, A. Moshnikova, D. M. Engelman, Y. K. Reshetnyak, O. A. Andreev, Probe for the measurement of cell surface pH in vivo and ex vivo. *Proc. Natl. Acad. Sci. U.S.A.* **113**, 8177–8181 (2016).
  35. R. Arppe, T. Näreaja, S. Nylund, L. Mattsson, S. Koho, J. M. Rosenholm, T. Soukka, M. Schäferling, Photon upconversion sensitized nanoprobe for sensing and imaging of pH. *Nanoscale* **6**, 6837–6843 (2014).
  36. J. S. Xie, H. Wu, C. Dai, Q. Pan, Z. Ding, D. Hu, B. Ji, Y. Luo, X. Hu, Beyond Warburg effect—Dual metabolic nature of cancer cells. *Sci. Rep.* **4**, 4927 (2014).
  37. J. Y. Lee, M. Onanyan, I. Garrison, R. White, M. Crook, M. F. Alexeyev, N. Kozhukhar, V. Pastukh, E. R. Swenson, C. T. Supuran, T. Stevens, Extrinsic acidosis suppresses glycolysis and migration while increasing network formation in pulmonary microvascular endothelial cells. *Am. J. Physiol. Lung Cell Mol. Physiol.* **317**, L188–L201 (2019).
  38. P. Swietach, S. Patiar, C. T. Supuran, A. L. Harris, R. D. Vaughan-Jones, The role of carbonic anhydrase 9 in regulating extracellular and intracellular pH in three-dimensional tumor cell growths. *J. Biol. Chem.* **284**, 20299–20310 (2009).
  39. H. Wu, V. Estrella, M. Beatty, D. Abrahams, A. El-Kenawi, S. Russell, A. Ibrahim-Hashim, D. L. Longo, Y. K. Reshetnyak, A. Moshnikova, O. A. Andreev, K. Luddy, M. Damaghi, K. Kodumudi, S. R. Pillai, P. Enriquez-Navas, S. Pilon-Thomas, P. Swietach, R. J. Gillies, T-cells produce acidic niches in lymph nodes to suppress their own effector functions. *Nat. Commun.* **11**, 4113 (2020).
  40. M. A. Proescholdt, M. J. Merrill, E.-M. Stoerr, A. Lohmeier, F. Pohl, A. Brawanski, Function of carbonic anhydrase IX in glioblastoma multiforme. *Neuro Oncol.* **14**, 1357–1366 (2012).
  41. J. Haapasalo, M. Hilvo, K. Nordfors, H. Haapasalo, S. Parkkila, A. Hyrsyluoto, I. Rantala, A. Waheed, W. S. Sly, S. Pastorekova, J. Pastorek, A.-K. Parkkila, Identification of an alternatively spliced isoform of carbonic anhydrase XII in diffusely infiltrating astrocytic gliomas. *Neuro Oncol.* **10**, 131–138 (2008).
  42. E. H. Ma, M. J. Verway, R. M. Johnson, D. G. Roy, M. Steadman, S. Hayes, K. S. Williams, R. D. Sheldon, B. Samborska, P. A. Kosinski, H. Kim, T. Griss, B. Faubert, S. A. Condotta, C. M. Krawczyk, R. J. De Berardinis, K. M. Stewart, M. J. Richer, V. Chubukov, T. P. Roddy, R. G. Jones, Metabolic profiling using stable isotope tracing reveals distinct patterns of glucose utilization by physiologically activated CD8<sup>+</sup> T cells. *Immunity* **51**, 856–870.e5 (2019).
  43. M. Rath, I. Müller, P. Kropf, E. I. Closs, M. Munder, Metabolism via arginase or nitric oxide synthase: Two competing arginine pathways in macrophages. *Front. Immunol.* **5**, 532 (2014).
  44. C. D. Mills, K. Kincaid, J. M. Alt, M. J. Heilman, A. M. Hill, M-1/M-2 macrophages and the Th1/Th2 paradigm. *J. Immunol.* **164**, 6166–6173 (2000).
  45. D. M. Hardbower, M. Asim, P. B. Luis, K. Singh, D. P. Barry, C. Yang, M. A. Steeves, J. L. Cleveland, C. Schneider, M. B. Piazuelo, A. P. Gobert, K. T. Wilson, Ornithine decarboxylase regulates M1 macrophage activation and mucosal inflammation via histone modifications. *Proc. Natl. Acad. Sci. U.S.A.* **114**, E751–E760 (2017).

46. K. Singh, L. A. Coburn, M. Asim, D. Barry, M. M. Allaman, C. Shi, K. Washington, A. P. Gobert, K. T. Wilson, Tu1857—Ornithine decarboxylase in macrophages exacerbates acute colitis and colitis-associated carcinogenesis by impairing M1 innate immune responses. *Gastroenterology* **154**, 51039 (2018).
47. D. J. Puleston, M. D. Buck, R. I. K. Geltink, R. L. Kyle, G. Caputa, D. O'Sullivan, A. M. Cameron, A. Castoldi, Y. Musa, A. M. Kabat, Y. Zhang, L. J. Flachsmann, C. S. Field, A. E. Patterson, S. Scherer, F. Alfai, F. Baixauli, S. K. Austin, B. Kelly, M. Matsushita, J. D. Curtis, K. M. Grzes, M. Villa, M. Corrado, D. E. Sanin, J. Qiu, N. Pällman, K. Paz, M. E. Maccari, B. R. Blazar, G. Mittler, J. M. Buescher, D. Zehn, S. Rospert, E. J. Pearce, S. Balabanov, E. L. Pearce, Polyamines and eIF5A hypusination modulate mitochondrial respiration and macrophage activation. *Cell Metab.* **30**, 352–363.e8 (2019).
48. C. Murdoch, M. Muthana, C. E. Lewis, Hypoxia regulates macrophage functions in inflammation. *J. Immunol.* **175**, 6257–6263 (2005).
49. J. Chiche, M. C. Brahimi-Horn, J. Pousysgur, Tumour hypoxia induces a metabolic shift causing acidosis: A common feature in cancer. *J. Cell. Mol. Med.* **14**, 771–794 (2010).
50. F. Okajima, Regulation of inflammation by extracellular acidification and proton-sensing GPCRs. *Cell. Signal.* **25**, 2263–2271 (2013).
51. P. C. Rodriguez, D. G. Quiceno, J. Zabaleta, B. Ortiz, A. H. Zea, M. B. Piazuelo, A. Delgado, P. Correa, J. Brayer, E. M. Sotomayor, S. Antonia, J. B. Ochoa, A. C. Ochoa, Arginase I production in the tumor microenvironment by mature myeloid cells inhibits T-cell receptor expression and antigen-specific T-cell responses. *Cancer Res.* **64**, 5839–5849 (2004).
52. S. Nagaraj, K. Gupta, V. Pisarev, L. Kinarsky, S. Sherman, L. Kang, D. L. Herber, J. Schneck, D. I. Gabrilovich, Altered recognition of antigen is a mechanism of CD8<sup>+</sup> T cell tolerance in cancer. *Nat. Med.* **13**, 828–835 (2007).
53. A. L. Chang, J. Miska, D. A. Wainwright, M. Dey, C. V. Rivetta, D. Yu, D. Kanojia, K. C. Pituch, J. Qiao, P. Pytel, Y. Han, M. Wu, L. Zhang, C. M. Horbinski, A. U. Ahmed, M. S. Lesniak, CCL2 produced by the glioma microenvironment is essential for the recruitment of regulatory T cells and myeloid-derived suppressor cells. *Cancer Res.* **76**, 5671–5682 (2016).
54. S. Ostrand-Rosenberg, C. Fenselau, Myeloid-derived suppressor cells: Immune-suppressive cells that impair antitumor immunity and are sculpted by their environment. *J. Immunol.* **200**, 422–431 (2018).
55. D. Bayik, Y. Zhou, C. Park, C. Hong, D. Vail, D. J. Silver, A. Lauko, G. Roversi, D. C. Watson, A. Lo, T. J. Alban, M. M. Graw, M. Sorensen, M. M. Grabowski, B. Otvos, M. A. Vogelbaum, C. Horbinski, B. W. Kristensen, A. M. Khalil, T. H. Hwang, M. S. Ahluwalia, F. Cheng, J. D. Lathia, Myeloid-derived suppressor cell subsets drive glioblastoma growth in a sex-specific manner. *Cancer Discov.* **10**, 1210–1225 (2020).
56. V. Kumar, S. Patel, E. Tcyganov, D. I. Gabrilovich, The nature of myeloid-derived suppressor cells in the tumor microenvironment. *Trends Immunol.* **37**, 208–220 (2016).
57. K. J. Svensson, J. E. Welch, P. Kucharzewska, P. Bengtson, M. Bjurberg, S. Pahlman, G. B. Ten Dam, L. Persson, M. Belting, Hypoxia-mediated induction of the polyamine system provides opportunities for tumor growth inhibition by combined targeting of vascular endothelial growth factor and ornithine decarboxylase. *Cancer Res.* **68**, 9291–9301 (2008).
58. T. F. Cloughesy, A. Y. Mochizuki, J. R. Orpilla, W. Hugo, A. H. Lee, T. B. Davidson, A. C. Wang, B. M. Ellingson, J. A. Rytlewski, C. M. Sanders, E. S. Kawaguchi, L. Du, G. Li, W. H. Yong, S. C. Gaffey, A. L. Cohen, I. K. Mellinshoff, E. Q. Lee, D. A. Reardon, B. J. O'Brien, N. A. Butowski, P. L. Nghiemphu, J. L. Clarke, I. C. Arrillaga-Romany, H. Colman, T. J. Kaley, J. F. de Groot, L. M. Liau, P. Y. Wen, R. M. Prins, Neoadjuvant anti-PD-1 immunotherapy promotes a survival benefit with intratumoral and systemic immune responses in recurrent glioblastoma. *Nat. Med.* **25**, 477–486 (2019).
59. K. Sakuishi, L. Apetoh, J. M. Sullivan, B. R. Blazar, V. K. Kuchroo, A. C. Anderson, Targeting Tim-3 and PD-1 pathways to reverse T cell exhaustion and restore anti-tumor immunity. *J. Exp. Med.* **207**, 2187–2194 (2010).
60. V. A. Levin, K. R. Hess, A. Choucair, P. J. Flynn, K. A. Jaecle, A. P. Kyritsis, W. K. A. Yung, M. D. Prados, J. M. Bruner, S. Ictech, M. J. Gleason, H.-W. Kim, Phase III randomized study of postradiotherapy chemotherapy with combination alpha-difluoromethylornithine-PCV versus PCV for anaplastic gliomas. *Clin. Cancer Res.* **9**, 981–990 (2003).
61. J. Zhao, A. X. Chen, R. D. Gartrell, A. M. Silverman, L. Aparicio, T. Chu, D. Bordbar, D. Shan, J. Samanamud, A. Mahajan, I. Filip, R. Orenbuch, M. Goetz, J. T. Yamaguchi, M. Cloney, C. Horbinski, R. V. Lukas, J. Raizer, A. I. Rae, J. Yuan, P. Canoll, J. N. Bruce, Y. M. Saenger, P. Sims, F. M. Iwamoto, A. M. Sonabend, R. Rabadan, Immune and genomic correlates of response to anti-PD-1 immunotherapy in glioblastoma. *Nat. Med.* **25**, 462–469 (2019).
62. E. A. Chiocca, J. S. Yu, R. V. Lukas, I. H. Solomon, K. L. Ligon, H. Nakashima, D. A. Triggs, D. A. Reardon, P. Wen, B. M. Stopa, A. Naik, J. Rudnick, J. L. Hu, P. Kumthekar, B. Yamini, J. Y. Buck, N. Demars, J. A. Barrett, A. B. Gelb, J. Zhou, F. Lebel, L. J. N. Cooper, Regulatable interleukin-12 gene therapy in patients with recurrent high-grade glioma: Results of a phase 1 trial. *Sci. Transl. Med.* **11**, eaaw5680 (2019).
63. A. J. Litterman, D. M. Zellmer, K. L. Grinnen, M. A. Hunt, A. Z. Dudek, A. M. Salazar, J. R. Ohlfest, Profound impairment of adaptive immune responses by alkylating chemotherapy. *J. Immunol.* **190**, 6259–6268 (2013).
64. N. J. MacIver, R. D. Michalek, J. C. Rathmell, Metabolic regulation of T lymphocytes. *Annu. Rev. Immunol.* **31**, 259–283 (2013).
65. E. T. Alexander, A. Minton, M. C. Peters, O. Phanstiel IV, S. K. Gilmour, A novel polyamine blockade therapy activates an anti-tumor immune response. *Oncotarget* **8**, 84140–84152 (2017).
66. U. Bachrach, The early history of polyamine research. *Plant Physiol. Biochem.* **48**, 490–495 (2010).
67. R. Poulin, A. E. Pegg, Stable intracellular acidification upon polyamine depletion induced by  $\alpha$ -difluoromethylornithine or  $N^1,N^{12}$ -bis(ethyl)spermine in L1210 leukaemia cells. *Biochem. J.* **312**, 749–756 (1995).
68. C. S. Hayes, A. C. Shicora, M. P. Keough, A. E. Snook, M. R. Burns, S. K. Gilmour, Polyamine-blocking therapy reverses immunosuppression in the tumor microenvironment. *Cancer Immunol. Res.* **2**, 274–285 (2014).
69. J. Miska, A. Rashidi, A. L. Chang, M. E. Muroski, Y. Han, L. Zhang, M. S. Lesniak, Anti-GITR therapy promotes immunity against malignant glioma in a murine model. *Cancer Immunol. Immunother.* **65**, 1555–1567 (2016).
70. J. W. Kim, J. Miska, J. S. Young, A. Rashidi, J. R. Kane, W. K. Panek, D. Kanojia, Y. Han, I. V. Balyasnikova, M. S. Lesniak, A comparative study of replication-incompetent and -competent adenoviral therapy-mediated immune response in a murine glioma model. *Mol. Ther. Oncol.* **5**, 97–104 (2017).
71. C. Lee-Chang, A. Rashidi, J. Miska, P. Zhang, K. C. Pituch, D. Hou, T. Xiao, M. F. Fischietti, S. J. Kang, C. L. Appin, C. Horbinski, L. C. Platanius, A. Lopez-Rosas, Y. Han, I. V. Balyasnikova, M. S. Lesniak, Myeloid-derived suppressive cells promote B cell-mediated immunosuppression via transfer of PD-L1 in glioblastoma. *Cancer Immunol. Res.* **7**, 1928–1943 (2019).
72. J. Miska, C. Lee-Chang, A. Rashidi, M. E. Muroski, A. L. Chang, A. Lopez-Rosas, P. Zhang, W. K. Panek, A. Cordero, Y. Han, A. U. Ahmed, N. S. Chandel, M. S. Lesniak, HIF-1 $\alpha$  is a metabolic switch between glycolytic-driven migration and oxidative phosphorylation-driven immunosuppression of tregs in glioblastoma. *Cell Rep.* **27**, 226–237.e4 (2019).
73. Z. B. Alfassi, On the normalization of a mass spectrum for comparison of two spectra. *J. Am. Soc. Mass Spectrom.* **15**, 385–387 (2004).
74. J. Chang, D. S. Wishart, J. Xia, Using MetaboAnalyst 4.0 for comprehensive and integrative metabolomics data analysis. *Curr. Protoc. Bioinformatics* **68**, e86 (2019).

**Acknowledgments:** We would like to thank Issam Ben-Sahra (Northwestern) for assistance in development and analyses of <sup>13</sup>C-flux studies. We would also like to thank the Tetramer core facility for the generation of OVA-specific tetramers. **Funding:** This work was supported by the Northwestern University RHLCCC Flow Cytometry Facility and a Cancer Center Support Grant (NCI CA060553) and an NIH/NINDS grant to both M.S.L. and J.M. (1R01NS115955-01), a grant from NIH/NINDS to M.S.L. (R01NS093903), and an Outstanding Investigator Award from NIH/NCI to N.S.C. (R35CA197532). J.M. also received a sub-award from (P50CA221747) SPORE for Translational Approaches to Brain Cancer, which supported this work. **Author contributions:** J.M., A.R., and M.S.L. conceived the study. J.M., A.R., C.L.-C., P.Z., R.B., S.S., B.C., D.H., A.C., and J.S.S. designed, performed, and analyzed experiments. A.L.-R. performed all animal breeding and genotyping for the study. P.G. performed all LC-MS/MS analyses. Y.H. provided assistance with animal surgeries and reagent preparations. T.X. performed and validated all statistical analyses. Y.K.R. synthesized and provided the pHLIP dye for ex vivo pH imaging. C.M.H. provided histological verification of data. M.S.L., N.S.C., M.B., and J.M. provided critical feedback, contributed to manuscript preparation, and oversaw the research program. All authors reviewed the manuscript and provided feedback with writing and revisions.

**Competing interests:** N.S.C. is on the scientific advisory board for Rafael Pharmaceuticals. Y.K.R. is the founder of pHLIP Inc. She has shares in the company, but the company did not fund any part of the work reported here, which was carried out in her academic laboratory and supported by NIH grant R01 GM073857. The authors declare no other competing interests.

**Data and materials availability:** All data needed to evaluate the conclusions in the paper are present in the paper and/or the Supplementary Materials. Additional data related to this paper may be requested from the authors.

Submitted 19 May 2020

Accepted 23 December 2020

Published 17 February 2021

10.1126/sciadv.abc8929

**Citation:** J. Miska, A. Rashidi, C. Lee-Chang, P. Gao, A. Lopez-Rosas, P. Zhang, R. Burga, B. Castro, T. Xiao, Y. Han, D. Hou, S. Sampat, A. Cordero, J. S. Stoolman, C. M. Horbinski, M. Burns, Y. K. Reshetnyak, N. S. Chandel, M. S. Lesniak, Polyamines drive myeloid cell survival by buffering intracellular pH to promote immunosuppression in glioblastoma. *Sci. Adv.* **7**, eabc8929 (2021).